University of Alberta

Library Release Form

Name of Author: Matthew Jason Atkins

Title of Thesis: Experimental Examination of the Effects of Fuel Octane and Diluent on HCCI Combustion

Degree: Master of Science

Year this Degree Granted: 2004

Permission is hereby granted to the University of Alberta to reproduce single copies of this thesis and to lend or sell such copies for private, scholarly, or scientific research purposes only.

The author reserves all other publication and other rights in association with the copyright in the thesis, and except as hereinbefore provided, neither the thesis nor any substantial portion thereof may be printed or otherwise reproduced in any material form whatever without the author's prior written permission.

_____

Matthew Jason Atkins

9638 72 Avenue

Edmonton, Alberta,

Canada, T6E 0Y6

"If we knew what it was we were doing, it would not be called research, would it?"

–Albert Einstein

University of Alberta

Experimental Examination of the Effects of Fuel Octane and Diluent on HCCI Combustion

by

Matthew Jason Atkins

A thesis submitted to the Faculty of Graduate Studies and Research in partial fulfillment of the requirements for the degree of Master of Science.

Department of Mechanical Engineering

Edmonton, Alberta

Fall 2004

University of Alberta

Faculty of Graduate Studies and Research

The undersigned certify that they have read, and recommend to the Faculty of Graduate Studies and Research for acceptance, a thesis entitled Experimental Examination of the Effects of Fuel Octane and Diluent on HCCI Combustion submitted by Matthew Jason Atkins in partial fulfillment of the requirements for the degree of Master of Science.

_____

Dr. C.R. (Bob) Koch (Advisor)

_____

Dr. Scott Meadows

_____

Dr. Brian Fleck

To my wife Georgia, who endured my late nights, soothed my anxieties and shared my enthusiasm. Thank you for your love, understanding and the countless personal sacrifices that you have made.

Abstract

Homogenous Charge Compression Ignition (HCCI) combustion promotes higher thermodynamic efficiencies and lower oxides of nitrogen emissions in internal combustion engines, when compared to spark ignition and compression ignition combustion processes. Experiments on a single cylinder engine are conducted to examine the effect of fuel octane and mixture dilution on HCCI. Engine parameters, cylinder pressure and exhaust emissions are measured for three Octane Numbers (ON) while varying Exhaust Gas Recirculation (EGR) and air/fuel ratio. Results show that both the Start of Combustion (SOC) and burn duration are best influenced using dilution, rather than ON. However, the ON is effective in increasing the HCCI load range. A comparison of excess air and EGR dilution shows that EGR is a more effective at controlling the SOC and burn duration. HCCI combustion can result in a highly efficient engine with very low oxides of nitrogen emissions while using a low octane fuel.

Acknowledgements

I would like to take this opportunity to acknowledge those who have made the completion of this thesis possible.

I wish to thank my supervisor, Dr. Bob Koch, for offering me the opportunity to do this degree. I am indebted to Dr. Koch for his vision, patience and technical guidance throughout the course of this work. I would further like to thank Dr. Koch for his financial support for the past two years.

I would like to express my gratitude to Dr. David Checkel, Dr. Doug Dale, and Mr. Mark Ackerman for their support and guidance.

Thanks are also due to the Mechanical Engineering machinist/technicians, Bernie Faulkner, Ian Buttar, Dave Pape, Rick Bubenko and Terry Nord for their expert skills and advice. Special thanks is due to Bernie Faulkner, for the help with my experimental setup.

Thanks to my colleagues in Room 2-14 and Room 5-29 for their support and many laughs.

Lastly, I would like to thank my family and my wife, Georgia, for supporting and encouraging me to pursue this degree.

TABLE OF CONTENTS

LIST OF TABLES

List of Figures

Nomenclature

Acronyms

AF . . . . Mass Air to Fuel Ratio

BMEP . . . . Brake Mean Effective Pressure

CAS . . . . Combustion Analysis System

CFR . . . . Cooperative Fuels Research (engine)

CI . . . . Compression Ignition

CO . . . . Carbon Monoxide

COV_{IMEP} . . . . Coefficient of Variance in IMEP

ECM . . . . Engine Control Module

EGR . . . . Exhaust Gas Recirculation

EOC . . . . End Of Combustion

FMEP . . . . Friction Mean Effective Pressure

HC . . . . Unburned Hydrocarbons

HCCI . . . . Homogenous Charge Compression Ig-
nition

Symbols

λ . . . . Lambda ($\lambda = \frac{AF_{actual}}{AF_{stoich}}$)

θ . . . . Crank angle

i . . . . Cylinder index

P . . . . Cylinder pressure

ΔP_c . . . . Pressure rise due to combustion

ΔP_c^* . . . . Corrected pressure rise due to combustion

V . . . . Cylinder volume

V_{TDC} . . . . Cylinder volume at TDC

$V_{iso-octane}$ . . . . Volume of iso-octane

$V_{n-heptane}$ . . . . Volume of n-heptane

k . . . . Polytropic index

m_{EGR} . . . . Mass of EGR

m_i . . . . Induced mass per cycle

r . . . . Volume fraction of exhaust gas in the reactants

r_{Eff} . . . . Effective dilution fraction

$m_{Excess\ Air}$ . . . . Mass of excess air

Chapter 1

Introduction

In most jurisdictions worldwide, legislation of emissions for new automobile engines are becoming ever more stringent. For example, the U.S. Environmental Protection Agency (EPA) Tier 2 program for new 2004 light duty vehicles, requires a reduction of 88 to 95% of Oxides of Nitrogen (NO_x) and at least an 80% reduction of Particulate Matter (PM) for the fleet average standard. One possible method that the internal combustion engine can meet the up coming emission levels is Homogeneous Charge Compression Ignition (HCCI) combustion. This chapter briefly describes the motivation for HCCI research, the problem statement, the organization of this thesis, and the contributions of this work.

1.1 Motivation

HCCI combustion has the potential to have high thermodynamic efficiency and to produce low emissions. HCCI engines can have efficiencies as high as Compression Ignition (CI) engines, while producing low NO_x and PM emissions [Iida et al., 2003]. Since, HCCI engines can operate on gasoline, diesel fuel, and most alternative fuels, it can be used with current fuel-refining capabilities. In addition, HCCI engines have the potential to be lower cost than CI engines because they could use a lower pressure fuel-injection system and the emissions control system would be less costly and less

dependent on scarce precious metals [DOE, 2001].

HCCI engines operate on the principle of having a homogeneous charge prepared either in the intake manifold or the cylinder by pre-mixing the fuel and air before the compression stroke of the engine. Then, if conditions are favorable, the pre-mixed charge auto-ignites during the compression stroke of the engine. The combustion occurs throughout the cylinder volume, without a flame front or a diffusion flame. However, the combustion rate is very fast and can potentially damage the engine [Oakley et al., 2001]. The combustion rate is reduced by diluting the air/fuel mixture with Exhaust Gas Recirculation (EGR) and/or excess air (lean operation).

HCCI combustion is achieved by controlling the temperature, pressure, and composition of the air/fuel mixture so that the ignition occurs spontaneously in the engine. This required control strategy is significantly more challenging than a Spark Ignition (SI) engine or CI engine because in HCCI combustion the Start of Combustion (SOC) is a complex function of chemical kinetics and not simply controlled by spark timing as in a SI engine or the injector timing as in a CI engine.

HCCI offers many benefits, but several technical challenges must be overcome to make HCCI engines suitable to a wide range of vehicles and viable for high volume production. A method of controlling SOC and burn duration over a range of engine speeds and loads must be determined. Currently, there are two distinct HCCI control strategies [Stanglmaier and Roberts, 1999]. The first strategy involves controlling the temperature of the air/fuel mixture. Increasing the temperature advances the SOC, and decreasing the temperature delays the SOC [Zhao et al., 2001]. The second strategy involves changing the auto-ignition properties of the air/fuel mixture. This can be done by fuel blending, adjusting the air/fuel ratio, or changing the amount of EGR in the cylinder. The air/fuel ratio and EGR affects the dilution of the air/fuel mixture. By increasing or decreasing the dilution, the SOC is delayed or advanced, respectively [Oakley et al., 2001]. The second challenge is that HCCI is limited to

low to medium loads due to the combustion rate. At high loads, the combustion process can become very rapid and intense causing unacceptable noise, potential engine damage, and eventually, high levels of NO_x emissions. The load range can be extended by using fuel blending, super-charging, or variable compression ratio engines. These methods can be used to extend the load obtainable by HCCI but for high load operation HCCI combustion is normally switched to SI or CI combustion. This allows the benefits of HCCI to be realized over a significant portion of the lower load driving cycle but requires the complexity of switching the engine between operating modes.

Numerous methods for controlling the SOC and burn duration and expanding the HCCI load range have been investigated, but no single method has yet to achieve all three objectives.

1.2 Problem Statement

The primary objective of this research is to experimentally examine the effect of fuel octane and mixture dilution on HCCI operating region, Indicated Mean Effective Pressure (IMEP), indicated specific NO_x emissions, indicated specific unburned Hydrocarbons (HC) emissions, indicated specific Carbon Monoxide (CO) emissions, Indicated Specific Fuel Consumption (ISFC), Start Of Combustion (SOC) and burn duration. The results are then used to show whether fuel Octane Number (ON) and dilution can be used to effectively influence the SOC, burn duration and HCCI load range.

1.3 Organization of Thesis

This thesis is organized into six chapters, including the introduction. Chapter 2 provides a detailed description of the fundamental principles behind HCCI, discusses previous related HCCI combustion studies and briefly describes the important features

of the experimental apparatus used in this research. A description of the fuel used in this study, a definition of misfire and knock boundaries, the method used to calculate the air/fuel ratio and percent EGR are discussed in Chapter 3. Also, detailed in Chapter 3 is the test procedure used to record data and how the SOC and burn duration are calculated. Chapter 4 discusses in detail the results for PRF20 and compares the results to other published HCCI studies. Then, the effect of ON on HCCI operating region, IMEP, indicated specific emissions(NO_x, HC, CO), ISFC, and SOC and burn duration is discussed. The various effects and benefits of ON on HCCI, the difference between excess air and EGR dilution and a correlation between ON, NO_x emissions and peak cylinder pressure is examined in Chapter 5. Finally, in Chapter 6, the main conclusions are presented and then potential methods on how the results here can be applied to HCCI operation in a vehicle are described. Then recommendations of future work and methods of improving the experimental setup are discussed.

1.4 Contributions

HCCI combustion experiments on a single cylinder engine using primary reference fuels with octane numbers of 20, 40 and 60, have been performed. A systematic variation of octane number has not (to my knowledge) been researched. The contributions of this thesis are as follows:

- HCCI combustion data at three fuel octane levels was experimentally documented. Engine parameters, exhaust emissions and cylinder pressure data was recorded for each operating point.

- Analysis of HCCI data was performed to determine whether the ON could be used to control the SOC and expand the HCCI load range. The analysis includes the effects of fuel ON and mixture dilution as a function of air/fuel ratio (λ)

and percent EGR on operating region, IMEP, indicated specific emissions (NO_x, HC, CO), ISFC, SOC and burn duration.

- Examination of the individual effects of dilution (λ and percent EGR) on the SOC and burn duration.

- The relation between indicated specific NO_x emissions as a function of fuel ON and peak cylinder pressure was correlated to provide insight into in-cylinder combustion conditions.

- Archiving high resolution cylinder pressure data at all operating points to provide a library of experimental data which can be used to validate HCCI chemical kinetic combustion models.

Chapter 2

Background

HCCI fundamentals, previous work on HCCI, the approach used in this thesis and a brief description of the experimental apparatus are subjects of this chapter.

2.1 HCCI Fundamentals

HCCI in an internal combustion engine is a combustion phenomena which uses a pre-mixed homogeneous air/fuel mixture that auto-ignites during the compression stroke. The basic HCCI operation concept is shown in Figure 2.1. Many researchers have described HCCI as a combination of SI and CI combustion [Aceves et al., 2001a, Christensen et al., 1997]. A homogeneous charge is prepared either in the intake manifold or in the cylinder, similar to a SI engine. Then, the pre-mixed charge auto-ignites during the compression stroke of the engine, similar to a CI engine. However, unlike a SI or CI engine in which the combustion occurs as a flame front or a diffusion flame, in HCCI combustion the charge effectively ignites simultaneously throughout the cylinder volume. The homogeneous mixture reduces NO_x and PM, caused by heterogeneous combustion. This combustion phenomenon is similar to knock in SI engines. The difference is that in knock, the end-gas that auto-ignites is a fraction of the original charge, where as in HCCI the entire charge auto-ignites. Much of the information from engine knock studies can be used in HCCI since engine knock has

6

many similar attributes to HCCI combustion.

(1) Intake of homogeneous air/fuel mixture

(2) The charge is compressed and the temperature increases

(3) Ignition occurs throughout the entire cylinder volume
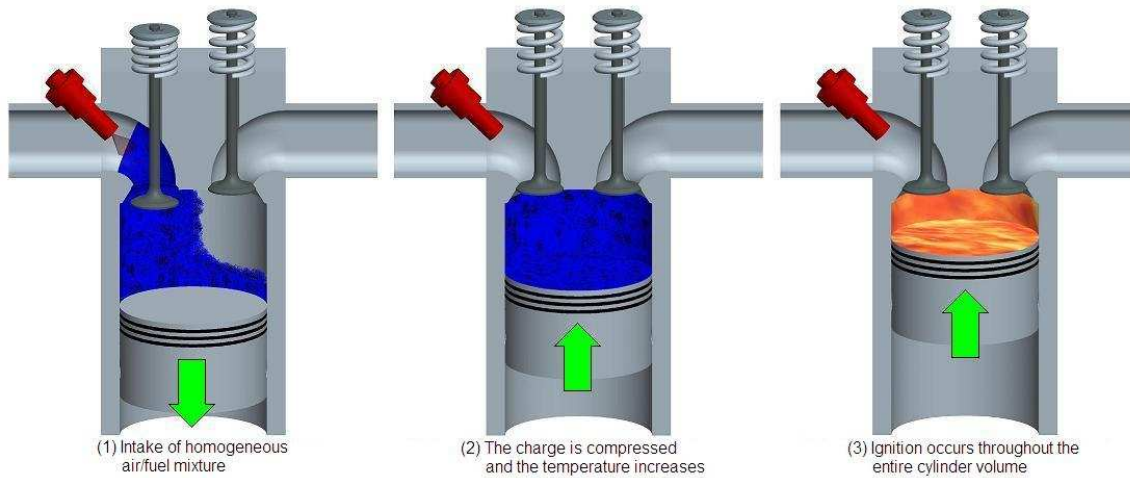
Figure 2.1: HCCI Operation

As in engine knock, the combustion rate of HCCI combustion can be very rapid or violent compared to a SI engine which can result in damage to the engine [Oakley et al., 2001]. To reduce the combustion rate the cylinder charge is diluted using EGR and/or excess air. This reduces the chemical energy of the mixture and slows the combustion rate. One result of the mixture dilution is that the HCCI load is limited to the low to medium load range. However, the dilution also allows the engine to be operated at wide open throttle, similar to a CI engine, which reduces pumping losses [Christensen et al., 1997] and significantly increases the engine efficiency.

Early studies in HCCI [Najt and Foster, 1983, Noguchi et al., 1979] found that the auto-ignition process of HCCI is controlled by chemical kinetics, with negligible influence from physical effects (turbulence, mixing). The chemical kinetics of an auto-igniting fuel consists of large numbers of simultaneous, interdependent reactions or chain reactions. Chain reactions are made up of initiating reactions where highly reactive intermediate species or radicals are produced from fuel and oxygen (Equation 2.1). Then the propagation reaction occurs where radicals react with reactant molecules to form products and other radicals (intermediates) to continue in the chain

reaction (Equation 2.2). These intermediate can either react to form stable molecules or active radicals. This is called degenerate branching (Equation 2.3). The chain reaction process ends with a termination reaction where the propagation radicals are removed (Equation 2.4). Below outlines the basic hydrocarbon (RH) oxidation process [Heywood, 1988].

$$RH + O_2 \rightarrow \dot{R} + H\dot{O}_2 \qquad \qquad Chain \quad Initiation \qquad (2.1)$$

$$\dot{R} + O_2 \rightarrow R\dot{O}_2$$
$$\dot{R} + O_2 \rightarrow olefin + H\dot{O}_2$$
$$R\dot{O}_2 + RH \rightarrow ROOH + \dot{R} \qquad Chain \quad Propagation \qquad (2.2)$$
$$R\dot{O}_2 \rightarrow R'CHO + R''O$$
$$H\dot{O}_2 + RH \rightarrow H_2O_2 + \dot{R}$$

$$ROOH \rightarrow R\dot{O} + \dot{O}H \qquad \qquad Degenerate \quad Branching \qquad (2.3)$$
$$R'CHO + O_2 \rightarrow R'\dot{C}O + H\dot{O}_2$$

$$R\dot{O}_2 \rightarrow destruction \qquad \qquad Chain \quad Termination \qquad (2.4)$$
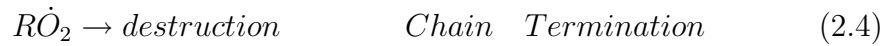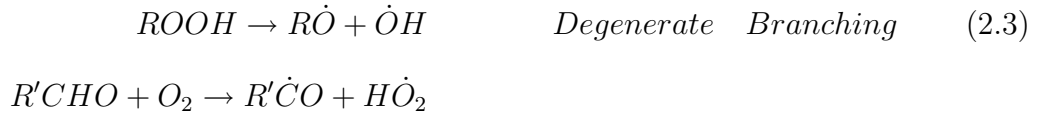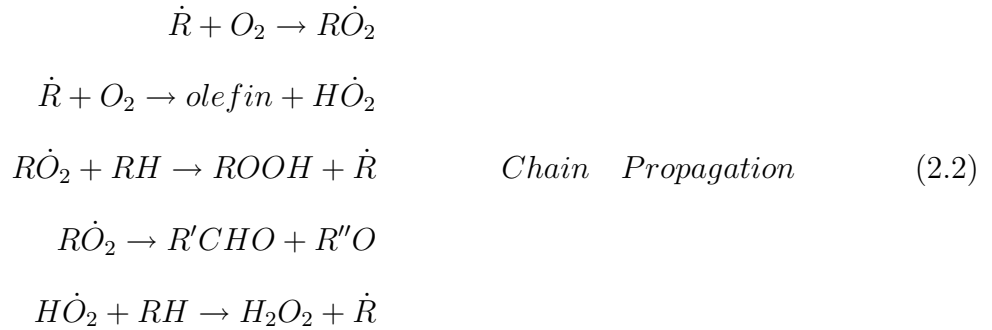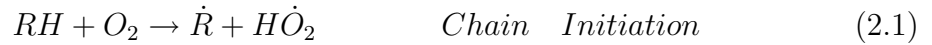
The dot indicates an active radical and the dash indicates the number of free bonds the radical has.

Chain initiation occurs at low temperature and produces radicals that start the chain propagation. The rate of chain propagation for straight-chain paraffins (n-heptane) is more intense than that of a branched chained paraffins (iso-octane). This is because a fuel that has long chained and many weakly bonded H atoms has a high isomerization rate, which leads to rapid ignition. For compact and highly branched

fuels with a large fraction of strongly bonded H atoms, isomerization and ignition is inhibited [Milovanovic and Chen, 2001].

The auto-ignition process starts when the heat energy released by the reactions is larger than the heat lost to the surroundings. The temperature of the mixture increases, which accelerates the rate of the reaction. As the temperature increases a point is reached where the mixture spontaneously ignites and the temperature and pressure rapidly increase.

The chain propagation, which controls the fuel auto-ignition, can exhibit two different phenomena. The first phenomena is called a two-stage ignition. As the temperature is increased to 300°C to 400°C a single or multiple cool flames occur. This phenomena is slightly exothermic and is quickly quenched by degenerative branching. However, the degenerative branching produces large numbers of OH radicals that react with fuel and subsequently increase the temperature of mixture. Once the temperature is over 1100K, the high temperature chain propagation takes place and quickly dominates the overall reaction which is the main ignition. The second phenomena has the same sequence, but the time to reach the high temperature chain propagation is considerably shorter and a cool flame is not observed. Both n-heptane and iso-octane have a main ignition that occurs at 1100K [Kelly-Zion and Dec, 2000], but n-heptane exhibits a two-stage ignition and iso-octane exhibits only a single stage ignition. The time required for main ignition depends on the heat release during the first stage of ignition, which determines the rate of temperature increase.

The auto-ignition process is dependent on the type of hydrocarbon. All hydrocarbons have a very rapid reaction rate after the main ignition, however, not all exhibit the initial cool flame ignition. Straight chained paraffins have strong a cool flame; however, branched chained paraffins are more resistant to cool flame behavior. The size of the molecule also affects the auto-ignition process, as methane does not exhibit the cool flame behavior and n-heptane does.

2.2 Previous HCCI Research

Controlling the Start of Combustion (SOC) and the combustion rate (burn duration) are essential in order to effectively use HCCI combustion in real engines. Two distinct control strategies can be used to control the SOC and combustion rate [Stanglmaier and Roberts, 1999]. First, the temperature of the air/fuel mixture can be controlled. Relatively simple methods use intake air heating or external EGR to heat the air/fuel mixture. More complex methods use a fully variable valve timing system to change valve overlap which changes the EGR rate, or use a variable compression ratio engine to change the peak cylinder pressure and temperature. Second, changing the auto-ignition properties of the air/fuel mixture can be used. This can be done by: fuel blending, or by adjusting the air/fuel ratio in conjunction with changing the percent EGR in the charge. By blending different fuels the auto-ignition properties of the air/fuel mixture can be changed to advance or delay the SOC. The air/fuel ratio and percent EGR affects the dilution of the air/fuel charge. By increasing or decreasing the dilution, the SOC is delayed or advanced, respectively [Oakley et al., 2001]. Using EGR as a diluent has some additional effects compared to excess air. The chemical species in EGR, such as carbon monoxide, hydrocarbons and hydroxyl radicals, can also affect the SOC and combustion rate, depending on the concentration of these species [Law and Allen, 2002].

The effect of changing the temperature of the air/fuel mixture by changing the intake air temperature and EGR for three different fuels, iso-octane, ethanol and natural gas was examined in Christensen and Johansson [1998]. The intake air temperature was adjusted to get the SOC to occur near Top Dead Center (TDC). They found that the use of EGR reduced combustion rate and retarded the SOC. They also showed that each fuel had its own auto-ignition properties and the combustion characteristics of each fuel responded slightly differently to intake air heating and

EGR.

Christensen et al. [1999] also demonstrated the potential of HCCI using a variable compression engine and intake air heating. The SOC can be adjusted to approximately TDC for all experiments by controlling compression ratio in conjunction with intake temperature. Tests were conducted with pure iso-octane, pure n-heptane, unleaded gasoline and diesel fuel. They demonstrated that nearly any liquid fuel can be used in an HCCI engine and it was possible to switch from pure iso-octane to pure n-heptane with the engine running.

The investigation of the HCCI operating region with respect to air/fuel ratio and EGR and their effect on IMEP, SOC, burn duration, ISFC, and indicated specific emissions were investigated by Oakley et al. [2001]. Experiments were conducted using gasoline (RON 95), at a fixed engine speed of 1500RPM, a fixed intake charge temperature of 320°C and a compression ratio of 11.5 to 1. They found that the HCCI operating region for unleaded gasoline was limited by three boundaries: misfire, partial burn, and knock limit. A similar study Peng et al. [2003] was conducted using n-heptane, at fixed engine speed of 1500RPM, a fixed intake charge temperature of 30°C and a compression ratio of 18 to 1. These studies showed that a wide operating region could be obtained with one fuel by using either high intake air temperature or high compression ratio. The SOC and combustion rate were shown to be a function of EGR and air/fuel ratio.

Zhao et al. [2002] studied the effect of EGR using a detailed chemical model which was validated with experimental results. EGR was separated into the following four factors: intake charge heating effect (hot EGR gases heat charge); dilution effect (reduction of oxygen in the charge due to EGR); thermal effect (higher specific heat capacity of EGR compared with air); and chemical effect (combustion products present in EGR can participate in chemical reactions). It was found that the SOC was predominately influenced by the thermal effect of EGR and the combustion duration

was mainly influenced by the thermal and dilution effects.

The effect of fuel composition on HCCI was examined by Aroonsrisopon et al. [2002]. The HCCI operating region of four different fuels was examined and it was found that the HCCI operating region differed significantly despite similar octane numbers for the four different fuels. The differences between the fuels was attributed to the fuel's individual auto-ignition chemistry.

In summary, the literature presents a good understanding of the effects of changing the temperature of the air/fuel mixture on HCCI combustion. However, the effect of ON on HCCI combustion and its utility in controlling the SOC and burn duration of HCCI has not been fully explored. Furthermore, experimental evaluation of the effectiveness of EGR and excess air as a diluent needs to be examined.

2.3 Approach Used

This study concentrates on experimentally examining the effect ON on HCCI combustion and how this can be used to control HCCI combustion using a single cylinder engine. The similarities and differences of using excess air or EGR as a diluent to influence HCCI combustion are also examined. The results reported here extend results in Oakley et al. [2001] by examining ON and with a more detailed investigation of mixture dilution. For three different octane numbers, the HCCI operating region, IMEP, indicated specific emissions (NO_x, HC, CO), ISFC, SOC and burn duration are investigated with respect to air/fuel ratio and percent EGR. The fuels used in this study are Primary Reference Fuels (PRF) with octane numbers of 20, 40 and 60. The auto-ignition properties of the air/fuel mixture are varied by changing the ON, the percent EGR and air/fuel ratio, while holding the intake temperature, engine speed and compression ratio constant. A correlation between NO_x emissions, ON and peak cylinder pressure is developed and discussed. Lastly, this study examines the effect

of EGR and excess air on the SOC and burn duration.

2.4 Experimental Apparatus

The engine used to research HCCI is a modified single-cylinder Co-operative Fuels Research (CFR) engine. The engine is outfitted with a port fuel injection system, a modified intake manifold, an optical encoder, a cylinder pressure transducer, and a wide range air/fuel ratio analyzer. The exhaust gases and intake air gases are analyzed by a six gas emission analyzer bench. The locations and interactions of the various components are depicted in Figure 2.2 and 2.3. Further details regarding the experimental apparatus are provided in Appendix A.

2.4.1 Fuel Injection System and Intake Manifold

The original intake manifold is replaced with a larger volume intake manifold that incorporates three fuel injectors near the intake port of the engine. The engine is setup with three injectors so that any combination of natural gas, hydrogen or gasoline can be used. The injectors are operated by a modified Sparrow Engine Control Module (ECM) from Alternative Fuel Systems. The ECM is capable of injecting two different fuels simultaneously at various pulse widths. This allows an easy transition from SI combustion to HCCI combustion. The fuel pulse width of each injector can be controlled by the operator, on fly with the SparroWatch program from a desktop PC. This allows the operator to control of the mass fuel rate and the mixture stoichiometry in the engine.

External EGR is routed into the intake manifold through a one inch diameter pipe, as shown in Figure 2.2. The EGR line emerges right behind the exhaust port and enters the midpoint in the intake manifold. This reduces EGR cooling and ensures that the EGR is well mixed with the fresh charge. The percent EGR is controlled

by adjusting a brass gate valve, located about midpoint in the EGR line. Fresh air entering the engine is heated by a 2kW air heater positioned upstream of the throttle body. The intake air heater is operated by a closed loop controller, in order to maintain the intake air at 88°C.

Figure 2.2: Engine Setup

2.4.2 Cylinder Pressure Transducer and Crank Angle Encoder

The cylinder pressure is measured with a Kisler water-cooled pressure sensor. The Kisler transducer is a piezoelectric pressure transducer. The operating principle is that the pressure acts on a diaphragm, which transfers this force to a quartz crystal. When the quartz crystal is put under load, the crystal produces an electrostatic charge that is proportional to the pressure change. An electrode transfers the charge to a charge amplifier, where it is integrated and converted into a positive voltage. This makes piezoelectric transducers very suitable for measuring the rapid, dynamic

pressure processes that occur in engines, however, they cannot be used for static pressures. The integration process requires that the charge amplifier periodically be reset to avoid drift. An optical encoder from BEI Industrial Encoders is connected

Figure 2.3: Instrumentation Setup

to the crankshaft on the front of the engine (Figure 2.3). The encoder provides 1/10 degree resolution on the angular position of the crankshaft. The encoder also produces one pulse per crankshaft revolution to provide a reference for each engine cycle. The output from both the cylinder pressure transducer and the encoder are used by a MTS Combustion Analysis System (CAS). The CAS provides, in realtime, combustion and engine operating parameters including: engine speed, IMEP, maximum pressure rise, peak pressure, peak pressure location and knock amplitude. The system is triggered to sample the pressure signal by the encoder, thus the pressure signal has 1/10 degree resolution. Statistical analysis of the pressure data is available from the CAS, including coefficient of variance of the IMEP, and percent misfires. The CAS is

connected to a PC through a TCP/IP network. The PC configures the CAS, displays the realtime data and stores the desired data.

2.4.3 Fast Air/Fuel Ratio Analyzer

A wide range air/fuel ratio analyzer from Engine Control and Monitoring is used to measure the air/fuel ratio without having to calculate the air/fuel ratio from the emission bench. The analyzer measures the air/fuel ratio using Universal Exhaust Gas Oxygen (UEGO) sensor. The UEGO sensor has a wide range (λ=0.4 to 10), fast response (<150ms) and is mounts directly in the engines exhaust. The electrochemical cell responds to O_2, CO, H_2, and HC in the exhaust to determine the air/fuel ratio (λ). The analyzer also has a programmable 0 to 5VDC analog output that is recorded by the data acquisition system.

2.4.4 Emission Analyzers

The exhaust gas composition is determined by using California Analytical Instruments emission analyzers. The emission bench included a paramagnetic oxygen (O_2) analyzer, a non-dispersive infrared carbon dioxide analyzer (CO_2) and carbon monoxide analyzer (CO), a flame ionization analyzer for total unburned hydrocarbon (HC), a heated flame ionization analyzer for unburned methane hydrocarbons (CH_4), and a chemiluminescence oxides of nitrogen analyzer (NO_x). The sample gas is filtered and cooled to remove any particulates and water from the sample gas prior to entering the analyzers in order to avoid incorrect readings and damaging the emission equipment. The emissions analyzers range and accuracy can be found in Appendix A.2.

CHAPTER 3

EXPERIMENTAL PROCEDURE

This chapter describes the fuels used in this study, and defines the misfire and knock boundaries. The method used to calculate air/fuel ratio and percent EGR is described as is the test procedure used to record data. Finally, a detailed description for calculating the SOC and burn duration is given.

3.1 Research Fuel

The auto-ignition behavior of HCCI combustion is similar to engine knock. Oppenheim [1984] defines knock as an undesirable mode of combustion that originates spontaneously and sporadically in the engine, producing sharp pressure pulses associated with a vibratory movement of the charge and the characteristic sound from which the phenomenon drives its names. A hydrocarbon's ability to resist auto-ignition or knock, depends on the fuel's molecular structure and size. Common fuels contain many individual hydrocarbons, such as paraffins, napthenes, olefins and aromatics, thus a property that indicates a fuel's resistance to auto-ignition is required. This property is defined by the fuel's ON. The ON scale is based on two PRF, n-heptane and iso-octane, which determine the start and end of the scale. Iso-octane has a high resistance to auto-ignition and has an ON of 100. With a low resistance to auto-ignition, n-heptane has an ON of zero. Blends of these two fuels, by volume, define

the auto-ignition resistance of intermediate ON.

$$ON = \frac{V_{iso-octane}}{V_{iso-octane} + V_{n-heptane}} \times 100 \qquad (3.1)$$

For example a blend of 20% iso-octane and 80% n-heptane has an ON of 20 and is called PRF20. The ON of other fuels is determined by measuring the blend of n-heptane and iso-octane that matches the other fuels knock qualities.

The fuels used in this study are blends of research grade iso-octane and n-heptane. Three different fuel blends are tested, PFR20 (ON 20), PFR40 (ON 40), and PFR60 (ON 60). The fuel properties used are shown below in Table 3.1. A high octane blend was also tested (PRF80), but, HCCI was not stable at the given operating conditions.

Table 3.1: Fuel Properties [Owen and Coley, 1990]

Property	PRF20	PRF40	PRF60
n-heptane (% volume)	80	60	40
iso-octane (% volume)	20	40	60
Octane Number (ON)	20	40	60
Density (kg/m^3)	689.6	691.2	692.8
Lower Heating Value (MJ/kg)	44.54	44.48	44.42
Higher Heating Value (MJ/kg)	48.04	47.98	47.92
Molecular Weight (kg/kmol)	103.0	105.8	108.6
Stoichiometric Air/Fuel Ratio	15.17	15.16	15.15

3.2 Defining Knock and Misfire Boundaries

The HCCI operating region is limited by two boundaries, misfire and knock (Figure 4.2). However, these boundaries are not the same for every study and must be defined. On a plot of air/fuel ratio (lambda) on the ordinate and percent EGR on the abscissa, the upper boundary or misfire boundary occurs at high air/fuel ratios or high EGR rates, when the charge is too diluted causing the occasional auto-ignition

failure. The misfire boundary is characterized by high CO and HC emissions and an increased Coefficient of Variance (COV_{IMEP}) in IMEP. The misfire boundary in this study is defined by the COV_{IMEP}. Drivability problems normally arise when the COV_{IMEP} exceeds 10% [Heywood, 1988]. Thus, the misfire boundary is defined to begin when the COV_{IMEP} exceeds 10%.

The knock boundary occurs at the lower boundary of the operating region. A standard method of characterizing knock does not seem to be established. Instead various methods have been developed, such as knock amplitude [Oakley et al., 2001, Peng et al., 2003], first derivative [Aroonsrisopon et al., 2002, Iida et al., 2003], and Root Mean Square (RMS) bandpass [Puzinauskas, 1992]. However, the knock threshold is still defined by an arbitrary number that is specific to that particular engine setup.

Oakley et al. [2001] and Peng et al. [2003] determine the knock threshold by bandpass filtering the pressure signal and then calculating the amplitude of the filtered signal. Next, they determine the Knock Occurrence Frequency (KOF) which is the percentage of cycles where the maximum amplitude of the filter signal is greater than 0.5bar. Engine knocking is defined, when KOF equals or exceeds 10%. Alternatively, Iida et al. [2003] and Aroonsrisopon et al. [2002] determined the knock threshold by calculating the first derivative of the pressure signal, with respect to the crank angle. They then define the knock limit where $\frac{dP}{d\theta}$ is greater than 10bar/deg. Since the first derivative is taken with respect to the crank angle and the combustion kinetics is partially governed by time, this method is sensitive to engine speed. Both of these methods were examined for uses in this study, however, the knock amplitude method limited the operating range to a very small area and the first derivative method was found to never exceed 10bar/deg. Thus, the above methods do not seem to generalize to the results reported in this study.

In this experiment the knock threshold is defined from the cylinder pressure, by

using the RMS bandpass method. The RMS bandpass method is used because it has low sensitivity to noise, it establishes the knock location and the knock number that is physically meaningful. The characteristic knock frequency for the CFR engine is approximately 5.1kHz. A fourth order Butterworth bandpass filter, with a cutoff frequencies of 3 and 8kHz, is used to filter out the low frequency component of pressure change due to combustion and filter out any high frequency noise. The resulting filtered signal is then analyzed. First, the signal RMS is calculated over a 10 degree window ending 15 degrees before peak cylinder pressure, to get the background RMS. Then the knock RMS is calculated for 10, 20, 30, 40, and 50 degree windows, after the peak cylinder pressure. The criteria for knock is defined to begin if the knock RMS value of a window exceeds four times the background RMS [Puzinauskas, 1992]. The knock level is identified relatively well using this method, but it is difficult to implement during testing. For testing the RMS bandpass method is correlated "by ear" to four audible knock levels. The human ear is a sensitive knock detector and is commonly used in determining octane requirements of fuels [Heywood, 1988]. The first level is "no knock" which indicates that there is no audible knock. The second level is "light knock" which indicates that there is a light ping audible from the engine. The third level indicates a "mild knock" which is an audible ping, but not overly loud. The fourth level is "heavy knock" which is a very audible ping and sounds almost destructive. Figure 3.1 shows the correlation between the RMS bandpass method and the audible knock levels. The 10 degree window is the most sensitive and the knock criteria corresponds to a "mild knock" audible level. Thus, for engine testing, the knock boundary is defined where the audible level is greater than the mild knock.
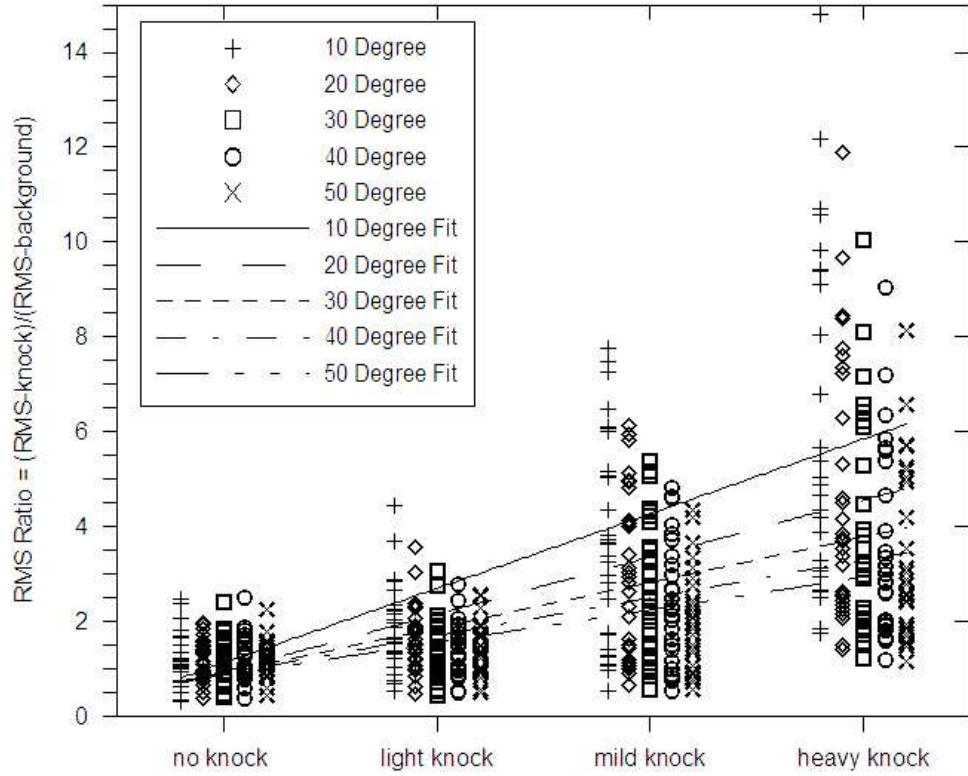
Figure 3.1: RMS Bandpass and Audible Knock Correlation

3.3 Emissions Calculations

The exhaust emissions concentration are used to calculate the air/fuel ratio and percent EGR. There are several methods to calculating the air/fuel ratio [Silvis, 1997] that require differing amounts of information from the gas concentration measurements. However, they all use the same basic chemistry of combustion. Here the method used to calculate the air/fuel ratio has the following conditions:

- changes the dry basis concentrations to wet basis concentrations

- accounts for the water in the air (humidity)

- accounts for any water left in the sample after the cooler

- assumes all NO_x is Nitric Oxide (NO)

- assumes that there is no hydrogen in the products

- assumes that fuel's hydrogen to carbon ratio is the same in the products as in the reactants

The basic unbalanced chemical equation for combustion is shown in Equation 3.2 [Silvis, 1997].

$$C_xH_yO_z + n(O_2 + A \cdot N_2 + B \cdot CO_2 + C \cdot H_{abs} \cdot H_2O) \rightarrow$$
$$aCO_2 + bCO + dH_20 + e0_2 + fN_2 + gNO_x + hC_{x'}H_{y'}O_{z'} \qquad (3.2)$$
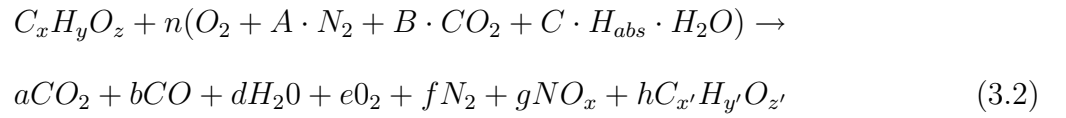
where the composition factors A, B, C and H_{abs} equal (note – [ ] indicates concentration by volume),

$$A = \frac{[N_2]_{amb}}{[O_2]_{amb}} \approx 3.774 \qquad B = \frac{[CO_2]_{amb}}{[O_2]_{amb}} \approx 0.16$$
$$H_{abs} = \frac{n_{H_2} \cdot 18.016}{n_{air} \cdot 28.96} \cdot 10^3 \qquad C = \frac{1.6076 \cdot 10^{-3} \times H_{abs}}{[O_2]_{amb}} \qquad (3.3)$$

Equation 3.2 does not include the EGR in the intake mixture. Heywood [1988] defines EGR as the percent of the total intake mixture which is recycled exhaust,

$$EGR(\%) = \frac{m_{EGR}}{m_i} \times 100 \qquad (3.4)$$

where m_{EGR} is the mass of the EGR and m_i is the inducted mass per cycle. If the EGR is assumed to be the same composition as the products, then the chemical

equation for combustion with EGR becomes,

$$C_xH_yO_z + n(O_2 + A \cdot N_2 + B \cdot CO_2 + C \cdot H_{abs} \cdot H_2O)+$$
$$r(aCO_2 + bCO + dH_2O + eO_2 + fN_2 + gNO_x + hC_{x'}H_{y'}O_{z'}) \rightarrow \quad (3.5)$$
$$aCO_2 + bCO + dH_2O + eO_2 + fN_2 + gNO_x + hC_{x'}H_{y'}O_{z'}$$
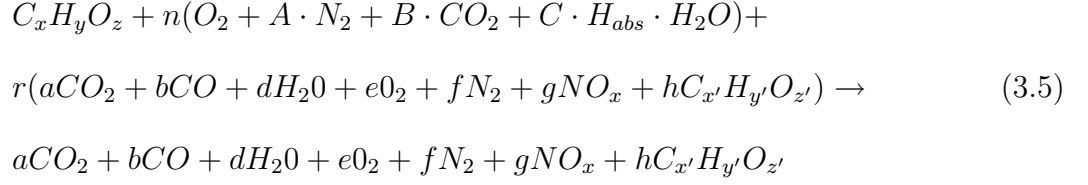
$$r = \frac{CO_{2_{Reactants}}}{CO_{2_{Products}}} \quad (3.6)$$

where r is the volume fraction of exhaust gas in the reactants. Since, the composition is the same, r can be determined by dividing the CO_2 concentration in the reactants by the CO_2 concentration in the products (Equation 3.6). With this method the CO_2 concentration in the products must be measured in order to calculate the percent EGR. A single CO_2 analyzer is used, with a two way solenoid valve, which allows both the exhaust gas composition and intake manifold composition to be measured. Normally, there is about 0.2% CO_2 already in the air and is accounted for by the B composition factor. However, since the CO_2 in the reactants is measured, the CO_2 in the air is accounted for and the B composition factor is set to zero. The CO_2 in the air, also results in the percent EGR never equalling zero.

The air/fuel ratio can be determined by conducting a carbon, hydrogen, oxygen and nitrogen balance with the measured coefficients a, b, e, g, h, and r. Then the percent EGR can be determined by calculating the mass of the recycled exhaust over the total mass of the reactants.

3.4 Test Procedure

The ambient temperature, wet bulb temperature and atmospheric pressure is measured prior to testing. The CFR engine is started and is warmed up for approximately one hour, until the engine oil, coolant and EGR reach the proper operating tempera-

ture (Table 3.2). During the warm up period, the CFR engine is fuelled with natural gas so that the engine can reach the proper operating temperature without knock occurring. The intake air heater is also turned on and the intake air temperature is gradually increased by the Programmable Temperature Controller until the intake air temperature is reached.

Table 3.2: Operating Conditions

Parameter	Operating Condition
Engine Speed	700RPM
Compression Ratio	12 to 1
Throttle Position	Wide Open Throttle (WOT)
Intake Air Temperature	88°C
Engine Oil Temperature	70°C
Coolant Temperature	96°C
Liquid Fuel Temperature	$\simeq$45 to 55°C
EGR Temperature	$\simeq$80 to 100°C

After the warm up period, the engine speed is set to 700RPM and the natural gas is replaced with the PRF blend. Once, the engine is operating entirely on the PRF and HCCI combustion is stable, the spark is turned off and testing can commence.

To record data, the percent EGR is set to the minimum rate and lambda is set to the knock boundary by changing the fuel pulse width. The throttle is always held wide open. Then the mass fuel rate is decreases incrementally, until the λ reaches the misfire boundary, with data being recorded at each increment. Then the percent EGR is increased approximately 2.5%, λ is moved back to the knock boundary and data is recorded again incrementally. This process is repeated until λ is stoichiometric at the knock boundary and the maximum percent EGR is achieved.

For each λ and EGR point the combustion is allowed to reach steady state before data collection occurs. This, generally requires about 30 to 40 seconds. Then the data collection begins by starting both the xPC data acquisition system and the CAS at the same time. The xPC system records the emissions concentrations, the mass air

flow, mass fuel flow, intake/exhaust manifold pressure, engine load and speed from the dynamometer, and λ from wide range air/fuel analyzer (Figure 2.3). The intake air temperature and exhaust temperature is also recorded by hand. Further details of the instrumentation and data acquisition system can be found in Appendix A. The CAS records the crank angle position and the cylinder pressure. The xPC system records data for 60 seconds, and the CAS records 50 engine cycles. The emission bench is switched manually from the exhaust CO_2 to the intake manifold CO_2 after 20 seconds has elapsed. This allows 115 engine cycles to be recorded from the exhaust, allows 20 seconds for the bench to reach steady state and allows 115 engine cycles to be recorded from the intake manifold. After each steady state operating point the data files names are recorded.

3.5 Start of Combustion and Burn Duration

The SOC is an important variable to control in a HCCI engine. In this study, the SOC is defined as the angular position of the crank shaft where 10% of the fuel is burned (CA10). Lower values (1%, 2% or 5%) of mass fraction could have been used in an attempt to capture the cool flame portion of the ignition, however, lower values are subject to larger errors [Oakley et al., 2001]. The Point Of Ignition (POI) and the End Of Combustion (EOC) are required in order to calculate the Mass Fraction Burned (MFB). The POI in a HCCI engine is not easy to identify, since unlike a SI engine with spark timing and a CI engine with injection timing to indicate the POI, a HCCI engine has neither of these indicators.

In this study the POI for HCCI combustion is determined by examining the concavity of a cylinder pressure curve. During the compression stroke the pressure curve is concave up and then changes to a concave down prior to reaching peak pressure. The concavity then switches back to concave up where the ignition occurs. Figure 3.2

shows the cylinder pressure and angular crank position for a typical measured HCCI operating point. The pressure signal clearly shows the concavity switching back to concave up at the POI, which is indicated by the '×' symbol.
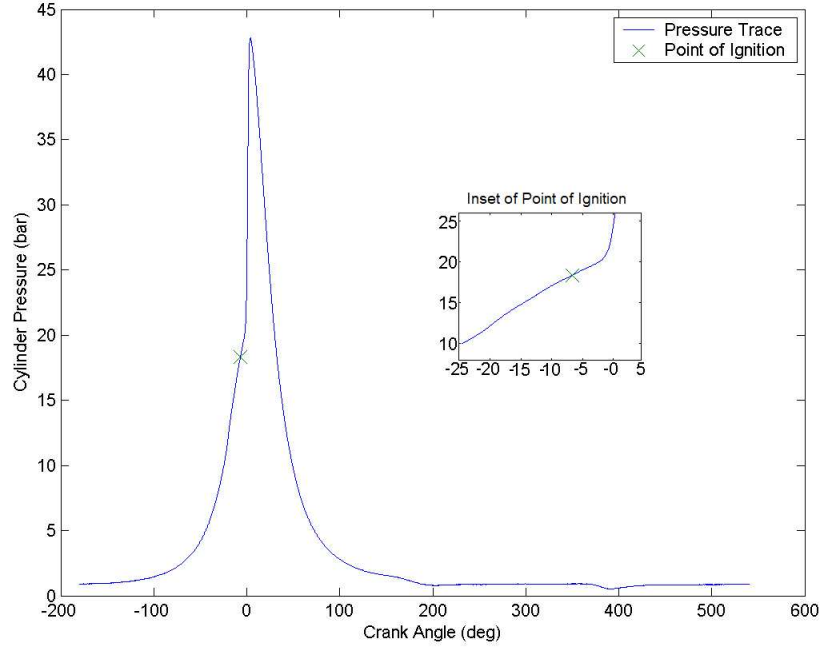
Figure 3.2: Point of Ignition, EGR=1.6%, λ=1.81

$$\frac{d^2P}{d\theta^2} > 0 \quad concave~up, \qquad \frac{d^2P}{d\theta^2} < 0 \quad concave~down \tag{3.7}$$

The second derivative of the pressure curve with respect to the crank angle determines whether the function is concave up or down (Equation 3.7). However, it is difficult to set criteria so that the POI can be found accurately using the second derivative. As a result, the third derivative of the pressure curve with respect to the crank angle is determined. The third derivative indicates the steepness of the rise of concavity and the point where combustion occurs causes the concavity to change rapidly. Thus, the POI can be found where the concavity rate of change becomes

very large.

Taking the third derivative of a measured signal requires a very low noise signal, particularly at high frequencies. This is obtained by averaging 50 engine cycles and filtering out high frequency noise. The POI is defined to be the first crank angle where the third derivative is greater than 2×10^{-5} [Kirchen, 2004] over a 30 degrees window starting 10 degrees before TDC. Other HCCI studies do not detail how the POI is determined.

The most common method of determining the EOC, is to determine the crank angle that provides a maximum value of x in Equation 3.8 over a five point summation [Brown, 2001]. To ensure that the EOC is not underestimated, ten degrees is added to the crank angle where x is a maximum.

$$x = \sum_{i=\theta-2}^{i=\theta+2} P_i V_i^{1.15} \tag{3.8}$$

Mass fraction burnt is a measure of the fraction of the energy released from combustion of the fuel to the total energy released at the end of the combustion process. It is determined from the analysis of measured cylinder pressure. There are several ways to calculate MFB, however, Rassweiler and Withrow [1938] developed a method in 1938 to calculate MFB that is still considered to be both accurate and computationally efficient (Equation 3.9). The pressure rise due to combustion (ΔP_c) is calculated from the difference between the incremental measured pressure rise and the pressure rise corresponding to a polytropic compression/expansion process. The pressure has to be corrected (ΔP_c^*) because the combustion does not occur at constant volume. It is corrected by referencing the pressure rise to cylinder clearance volume at TDC,

V_{TDC}.

$$\Delta P_c^* = \left[P_{i+1} - P_i \left(\frac{V_i}{V_{i+1}} \right)^k \right] \frac{V_i}{V_{TDC}} \tag{3.9}$$

Then the MFB for a given angle is given by:

$$MFB_\theta = \frac{\sum\limits_{POI}^{\theta} \Delta P_c^*}{\sum\limits_{POI}^{EOC} \Delta P_c^*} \tag{3.10}$$

Figure 3.3 shows the MFB for a HCCI operating point at EGR=1.6% and λ=1.81. The POI occurs at -6.7 degrees, the SOC is at MFB=0.1 or -0.7 degrees and the burn duration is the difference between MFB=0.9 and MFB=0.1, or 3.2 degrees. The burn duration of a HCCI engines is much faster than for a SI engine. A SI engine operating at 1500RPM, EGR=0% and λ=1.0, has a 10 to 90% burn duration of 17 degrees [Heywood, 1988]. Therefore, the percentage of the mass fraction burnt is rather important due to the rapid burn duration of HCCI combustion. Figure 3.3 shows that the sensitivity of the crank angle dramatically increases for MFB less than 10%, or greater than 90%. Thus, studies such as Zhao et al. [2001] that use MFB of 5% to 90% will have higher burn duration than the results presented here.
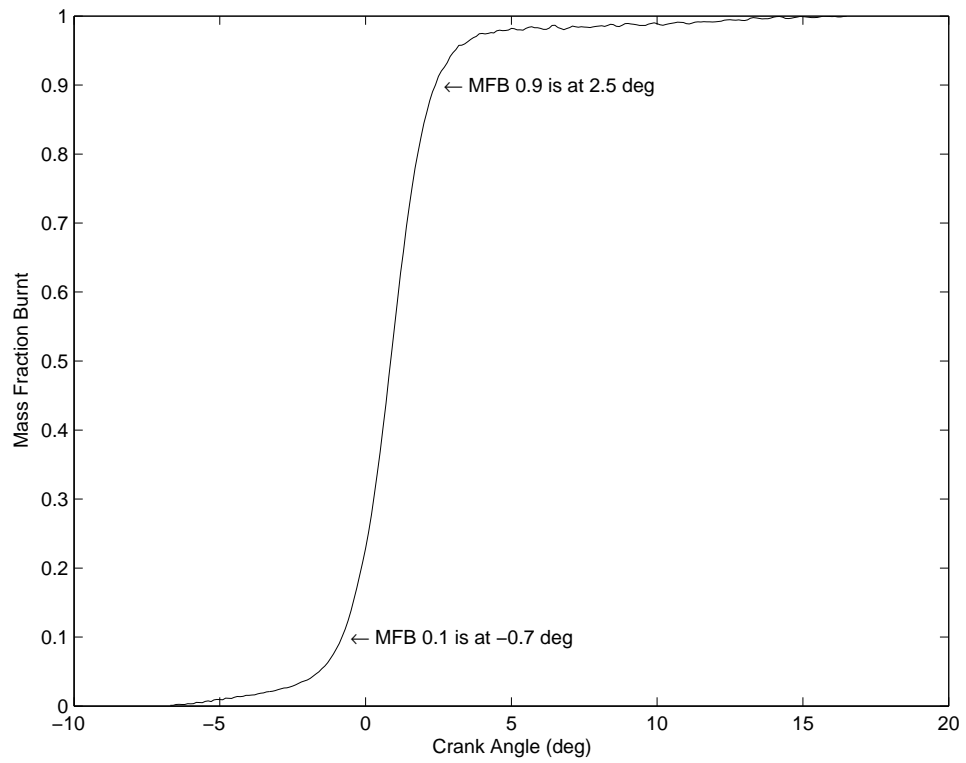
Figure 3.3: Mass Fraction Burnt, EGR=1.6%, λ=1.81, 700RPM (crank angle is relative to TDC)

Chapter 4

Experimental Data

In this section the experimental uncertainty is presented in order to put the results in context. Then the experimental results for the PRF20 fuel are presented and compared to published results. Lastly, the effect of ON on operating region, IMEP, indicated specific emissions (NO_x, HC, CO), ISFC, SOC and burn duration are examined.

4.1 Experimental Uncertainty

To estimate experimental uncertainty, the entire test matrix for each of the three fuel ON was repeated on three different occasions. At any given operating point the average and maximum standard deviation for engine parameters, emission measurements, and combustion parameters is given in Table 4.1. Outlier points that resulted from the occasional measurement error have been removed from the results in Table 4.1. The average and maximum standard deviation for each parameter is determined by comparing five similar points from each of the three PRF20 data sets. First the standard deviation between three data sets for that individual parameter is determined. Then the average and maximum standard deviation of the five similar data points is determined. The average and maximum standard deviation in Table 4.1 is slightly inflated because the EGR and λ for each of the five similar data points is not exactly

Table 4.1: Experimental Uncertainty for PRF20

Parameter	Average Standard Deviation	Maximum Standard Deviation
EGR	6.2%	17.3%
λ	2.6%	6.4%
IMEP	3.7%	5.6%
NO_x	14.3%	22.5%
HC	11.7%	20.0%
CO	10.1%	16.7%
ISFC	7.0%	10.7%
SOC	1.9 degrees	3.1 degrees
Burn Duration	18.0%	25.3%

the same. EGR and λ have an average standard deviation of 6.2% and 2.6%, respectively. Thus, the exact same points are not compared. This is particularly evident by parameters that are very sensitive to small changes in EGR or λ, such as SOC, burn duration and NO_x. Nevertheless, a measure of how repeatable the steady state operating points is gained.

The POI, SOC and burn duration mean and standard deviation of 50 engine cycles for a single HCCI data point (EGR=2.3%, λ=1.99) is shown in Table 4.2. The corresponding cylinder pressure versus crank angle of the 50 engine cycles is shown in Figure 4.1, where the '×' indicates the POI. The standard deviation of the POI is relatively large compared to the SOC and burn duration. The POI is determined by calculating the third derivative of the pressure signal (Section 3.5). This make the POI very sensitive to signal noise. Alternatively, the SOC and burn duration, determined from the mass fraction burned, are smooth due to the integrating effect of the equation and as a result are less sensitive to signal fluctuations and noise. Thus, for comparison between operating points, SOC is a better measure than POI of when the combustion starts. Figure 4.1 shows that there is relatively little variation from cycle-to-cycle, however, the POI does exhibit larger variations.

Table 4.2: Cycle-to-Cycle Variation, EGR=2.3%, λ=1.99

	POI (deg)	SOC (deg)	Burn Duration (deg)
Mean	-7.5	3.71	4.46
Standard Deviation	5.4	0.57	0.36
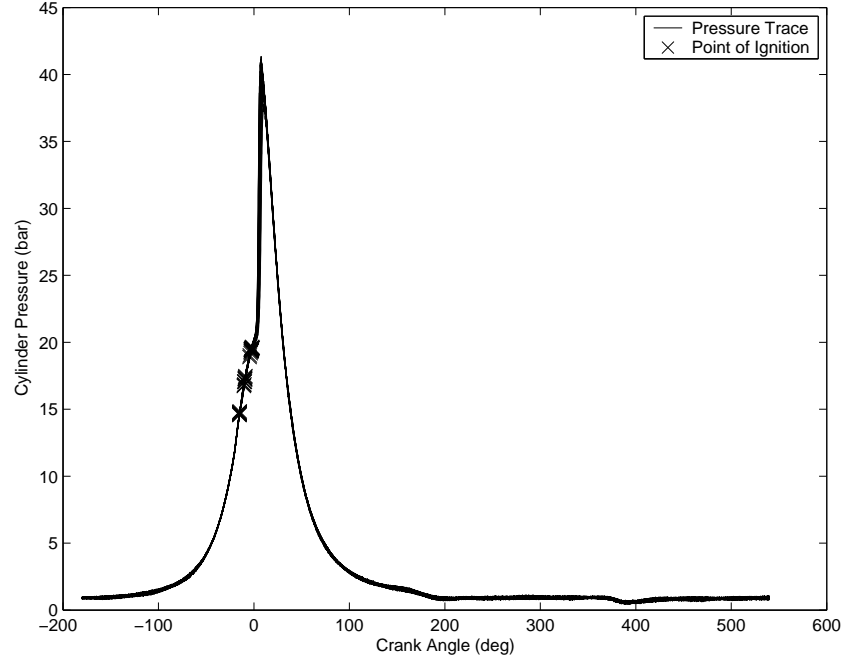
Figure 4.1: Cycle-to-Cycle Variation, EGR=2.3%, λ=1.99

4.2 PRF20

4.2.1 Operating Region

Figure 4.2 shows the HCCI operating region. The operating region is plotted as a function of EGR on the x-axis and λ on the y-axis. The 'o' symbols represent experimentally measured data points. The lower line represent the knock boundary and upper line represents the misfire boundary. For this engine, HCCI operation is possible only between the boundary lines.

The operating region is a diagonal band shape, which starts at minimum EGR/ maximum λ and angles downward to maximum EGR/minimum λ. This shape occurs

because the mixture must be diluted to prevent excessive knock but too much dilution results in a failure to auto-ignite. Thus, the operating region is a balance of dilution between λ and EGR.

The operating regions in Oakley et al. [2001] and Peng et al. [2003] exhibit a similar shape and have similar operating boundaries, but both studies have a much larger operating region. The intake air temperature and/or compression ratio are higher in these studies allowing a greater range where the mixture can auto-ignite.

The air/fuel ratio gives a measure of how much excess air dilution is in the mixture, however, it does not include the EGR dilution. To examine the effects of dilution as a whole, it is necessary to define a dilution parameter that includes both excess air and EGR. In this study it is defined as effective dilution (r_{Eff}) which is the sum of the mass of EGR and mass of excess air for each operating point divided by stoichiometric mass of the air/fuel mixture (Equation 4.1).

$$r_{Eff} = \frac{m_{EGR} + m_{Excess\,Air}}{m_{Stoichiometric}} \qquad (4.1)$$

Figure 4.3 shows the effective dilution map for the PRF20. (Note - Some of the features of the contour plots may be due to the interpolation algorithm used for plotting or due to experimental error.) The effective dilution decreases as the EGR is increased. This indicates that excess air and EGR do not have the same dilution effect. This is consistent with other studies that show EGR is not just an inert diluent, but also has thermal and chemical effects [Zhao et al., 2001]. This indicates that less EGR by mass is required to control HCCI between the knock and misfire boundary compared to excess air.

In this study, the engine is operated at WOT, constant engine speed and the fuel is adjusted to change the air/fuel ratio and regulate the power output. Thus, the cylinder inducts approximately the same total mass of fresh air and/or EGR

every cycle. Therefore, the primary effect of the dilution is that it reduces flame temperatures and the combustion rate by reducing the total energy in the cylinder charge.

4.2.2 Indicated Mean Effective Pressure

The IMEP map, plotted as a function of EGR and λ, is shown in Figure 4.4. The IMEP is a maximum of 5.0bar near the stoichiometric conditions ($\lambda = 1$) because the dilution is a minimum, and the IMEP is a minimum of 3.5bar at maximum λ ($\lambda = 2.6$) because the dilution is a maximum. For most of Figure 4.4, IMEP decreases as the mixture dilution is increased. Near the knock boundary however, IMEP exhibited slightly different behavior. This behavior is not really apparent in Figure 4.4, but is evident in the IMEP maps for the PRF40 and PRF60 fuels (Figures 4.13 and 4.22). The IMEP increases slightly as the operating points become leaner and move away from the mild knock boundary. This increase occurs between the knock boundary and approximately one tenth λ above the knock boundary. This differs from other studies and is attributed to the mild knocking which causes increased heat transfer to the piston and cylinder walls [Heywood, 1988] resulting in a slightly lower IMEP at the knock boundary.

4.2.3 Indicated Specific Emissions

The emission concentration are measured in parts per million (ppm), however, normalized indicators of emissions levels are more useful for comparison purposes. Indicated specific emissions are the mass flow rate of the species per unit of indicated power (Equation 4.2).

$$iSpecies = \frac{\dot{m}_{Species}}{P} \qquad (4.2)$$

Oxides of Nitrogen Emissions

Figure 4.5 shows the effect of EGR and air/fuel ratio on indicated specific NO_x. All the NO_x emissions for the PRF20 are small compared to an SI Engine. For a typical SI engine, at a load of 4.0bar, indicated specific NO_x is approximately 13g/kWhr [Oakley et al., 2001], while at a same load, the NO_x is 0.05g/kWhr for HCCI combustion.

In this thesis, NO_x emissions are highest (1g/kWhr) at the knock boundary and are lowest (0.05g/kWhr) at the misfire boundary. In Figure 4.5 the contour iso-lines are almost parallel to the boundaries, thus the NO_x decreases as the dilution increases with either λ or EGR. The combination of a homogeneous and diluted mixture results in low NO_x emissions. The homogeneous mixture prevents NO_x formation due to localized hot spots (heterogenous combustion) and the dilution lowers the combustion temperature below 1800K where NO_x formation becomes significant [Christensen et al., 1997].

The NO_x emissions exhibit a slightly different trend near stoichiometric conditions. The iso-lines become vertical and curve into the knock boundary. This trend occurs because the increased oxygen concentration offsets the reduction in combustion temperature in the formation of NO_x as the mixture becomes leaner. Heywood [1988] indicates that the NO_x emissions are affected by combustion temperature greater than $\lambda = 1.11$ and affected by increased oxygen concentration between $\lambda = 1$ and $\lambda = 1.11$.

Unburned Hydrocarbon Emissions

The indicated specific HC emission map for the PRF20 is shown in Figure 4.6. As expected, the HC emissions are a minimum (18g/kWhr) near the knock boundary where the combustion temperature are the highest, and are a maximum (32g/kWhr) near the misfire boundary where combustion temperatures are lowest. The HC emissions are also slightly lower near stoichiometric condition with high EGR levels than

at lean conditions with low EGR.

The most significant source of the HC emissions in HCCI combustion is incomplete combustion in the crevices and near walls where the mixture temperature is cooler. For higher load operating conditions, both experimental and computation results support this hypothesis [Aceves et al., 2001b, Christensen and Johansson, 2001]. However, for light load conditions (IMEP < 3.0bar) or high dilution ($\lambda \geq 4.5$), the dominate source of HC and CO emissions is from incomplete bulk-gas reactions [Dec and Sjöberg, 2003]. This occurs because at high dilution levels the combustion temperatures are too low to complete the reaction before expansion. Since the minimum IMEP in this study is 3.6bar, the HC emissions are caused by incomplete combustion in the crevices and/or near cylinder walls.

The HC emissions increase as the mixture becomes more diluted because the combustion temperature decreases and less of the HC is oxidized. The HC emissions are also lower near stoichiometric because the dilution is at a minimum, resulting in higher combustion temperatures.

The HC emissions trends in this study are similar to the results reported in Oakley et al. [2001], except here the magnitude of the HC emissions are much lower. In Oakley et al. [2001], the engine was operated into the partial burn region where combustion quality deteriorates. The engine in this study could not be operated in the partial burn region due to the comparatively low intake air temperature (88°C versus 320°C [Oakley et al., 2001]). The HC emissions are therefore much lower in this study.

Carbon Monoxide Emissions

The CO emissions are a minimum (8g/kWhr) near the knock boundary, where the combustion temperature are the highest, and are a maximum (20g/kWhr) near the misfire boundary (Figure 4.7). Also, the CO emissions are lower near stoichiometric condition than at lean conditions with low EGR.

Similar to the HC emissions, the main source of CO emissions at high load conditions is from incomplete combustion in the crevices and/or near walls where the mixture temperature is cooler [Aceves et al., 2001b, Christensen and Johansson, 2001]. At light loads, Dec and Sjöberg [2003] found that CO emissions are very sensitive to the bulk-gas reaction completeness occurring when the combustion temperature in the bulk-gas reaction is too low to complete the CO-to-CO_2 reaction. In this study, the engine load is higher than the engine load found in Dec and Sjöberg [2003], therefore, most of the CO emissions are from incomplete combustion in the crevices and/or near walls.

The CO emissions increase as the mixture becomes more diluted because the combustion temperature decreases. This results in less of the CO oxidizing to CO_2, particular in the crevices and near the cylinder walls where the combustion temperatures are even lower. At stoichiometric conditions the dilution level is lower than at high λ conditions which results higher combustion temperatures and lower CO emissions.

The CO emissions in Oakley et al. [2001] are significantly higher than in this thesis, although the CO emission trends are similar. The higher CO emissions in Oakley et al. [2001] are due to the engine was operated into the partial burn region where combustion quality deteriorates. As indicated above, the engine in this study could not be operated in the partial burn region therefore the CO emissions are much lower in this study.

4.2.4 Indicated Specific Fuel Consumption

ISFC is a measure of how efficiently the engine uses the fuel supplied to do work. It is defined as the fuel mass flow rate divided by the indicated power (Equation 4.3).

$$ISFC = \frac{\dot{m}_{Fuel}}{P} \tag{4.3}$$

At a load of 5.7bar this engine has an ISFC of 325g/kWhr in SI Mode (PRF20), compared to 265g/kWhr in HCCI mode (PRF60). This is an 18% improvement in ISFC.

In HCCI operation ISFC decreases as the mixture becomes more diluted, either with λ or EGR as shown in Figure 4.8. The ISFC decreases with increased dilution for two reasons. First, the heat loss to the cylinder walls is reduced because the combustion temperatures are reduced. Second, the dilution reduces the degree of dissociation in the high-temperature burned gases which allows more of the fuels energy to be converted to sensible energy near TDC [Heywood, 1988]. Hence a greater fraction of the fuel's energy is transferred as work to the piston and less energy is rejected to the exhaust.

The minimum ISFC for the PRF20 case occurred at high EGR levels near stoichiometric (230g/kWhr) and the maximum ISFC occurred along the upper half of the misfire boundary (280g/kWhr). However, Figure 4.3 shows that the effective dilution is a minimum near stoichiometric conditions where the minimum ISFC occurs. For this engine, despite operating at WOT, increasing the percent EGR increases the intake manifold pressure slightly (reduces vacuum) which reduces the engines pumping losses. This effect contributes to decreasing ISFC as EGR is increased.

The ISFC trend found in this study is different from the results found in Oakley et al. [2001] and Peng et al. [2003]. Both of these studies indicate that the ISFC increases as λ increases and is nearly constant with EGR. The difference between this

work and Oakley et al. [2001] and Peng et al. [2003] is the amount of dilution. In general, as λ increases the ISFC decreases due to less heat transfer to the cylinder walls and due to more of the chemical energy being converted to work. However, the ISFC eventually reaches a minimum and further increasing λ causes the cycle-to-cycle pressure fluctuation and the burn duration increase. Both of these factors degrade the engine efficiency, resulting in ISFC to increase. In Oakley et al. [2001] and Peng et al. [2003] the engines were operating lean of the minimum ISFC which results in the ISFC increasing as the dilution increases. In this study, the engine is operating rich of the minimum ISFC resulting in ISFC decreasing as dilution is increased.

4.2.5 Start of Combustion and Burn Duration

The SOC map for the PRF20 is presented in Figure 4.9. In this study, the SOC is defined as the crank angle where 10% of the fuel has burned. The burn duration map for the PRF20 is presented in Figure 4.10. The burn duration is defined as the crank angle where 10% to 90% of the fuel has burned.

The SOC iso-lines are nearly parallel with the knock and misfire boundaries. The minimum SOC occurs slightly before TDC (-2 degrees) near the knock boundary, however, increases to a maximum of 10 degrees after TDC near the misfire boundary. The burn duration iso-lines are also nearly parallel to the boundary limits. The burn duration near the knock boundary varies between 3 and 4 degrees while near the misfire boundary it varies between 10 and 15 degrees. Both the SOC and burn duration are found to be greatly influenced by the mixture dilution.

Increasing λ causes the SOC to occur slightly later and the burn duration becomes longer. A lower end-of-compression temperature and pressure due to a higher specific heat capacity of the leaner mixture [Zhao et al., 2001] is thought to cause this.

The effect of EGR on SOC can be divided into dilution, thermal and chemical effects [Zhao et al., 2001], however, the thermal effect has the most significant influ-

ence. The thermal effect is caused by some O_2 in the mixture being replaced with CO_2 and H_2O which increases the specific heat capacity of the mixture. This results in a slightly lower temperature at the end of the compression stroke and delays the SOC to when the charge reaches the proper ignition temperature. This is shown in Figure 4.9 where the SOC increases with increasing EGR.

The burn duration is also influenced by dilution, thermal and chemical EGR effects [Zhao et al., 2001]. Increasing EGR extends the burn duration because the thermal effect reduces the combustion temperature and the dilution effect reduces oxygen availability. However, the chemical effect reduces the burn duration as EGR is increased by producing extra O and OH due to the decomposition of CO_2 and H_2O. The combined effect of EGR is that the burn duration increases for increasing EGR levels, as shown in Figure 4.10.

4.2.6 Figures - PRF20
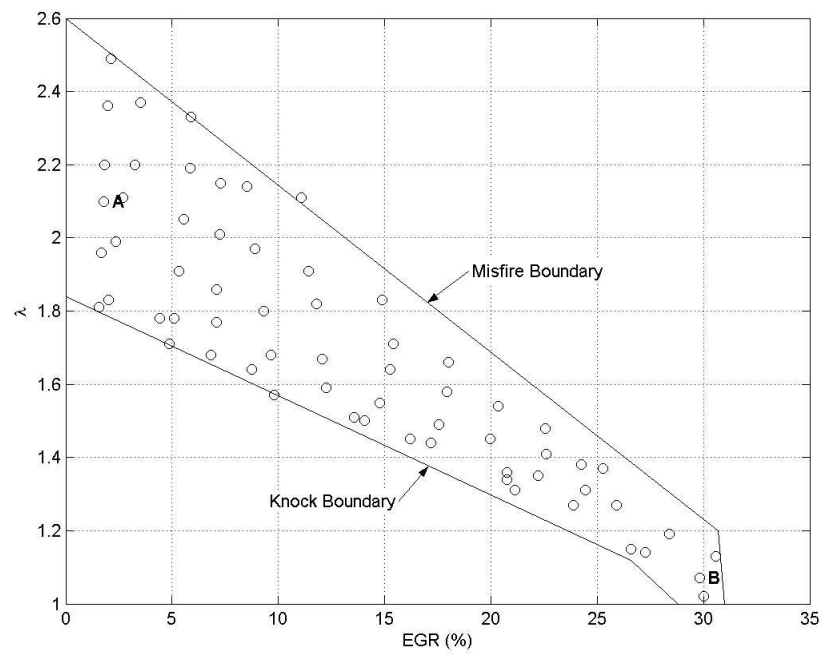
Figure 4.2: HCCI Operation Region for PRF20
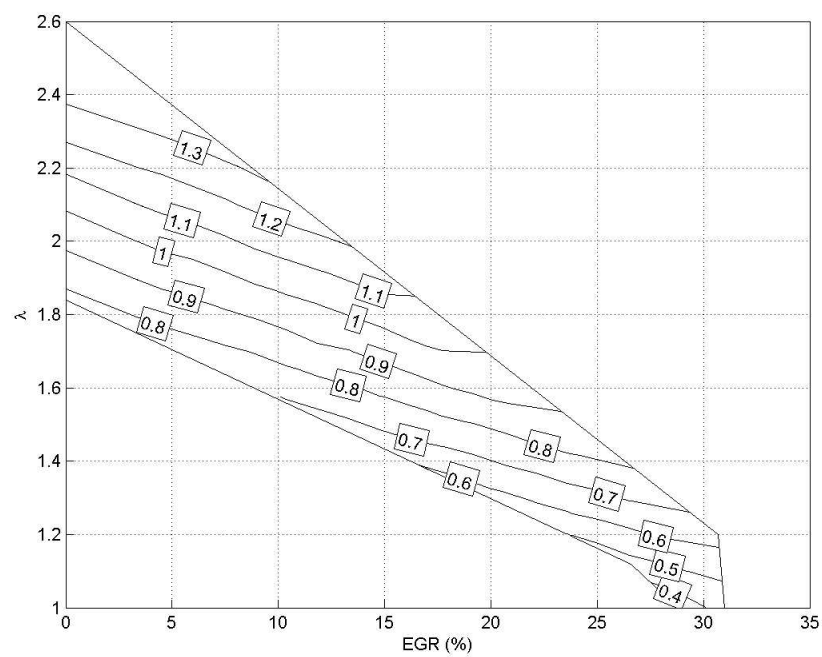
Figure 4.3: Effective Dilution for PRF20
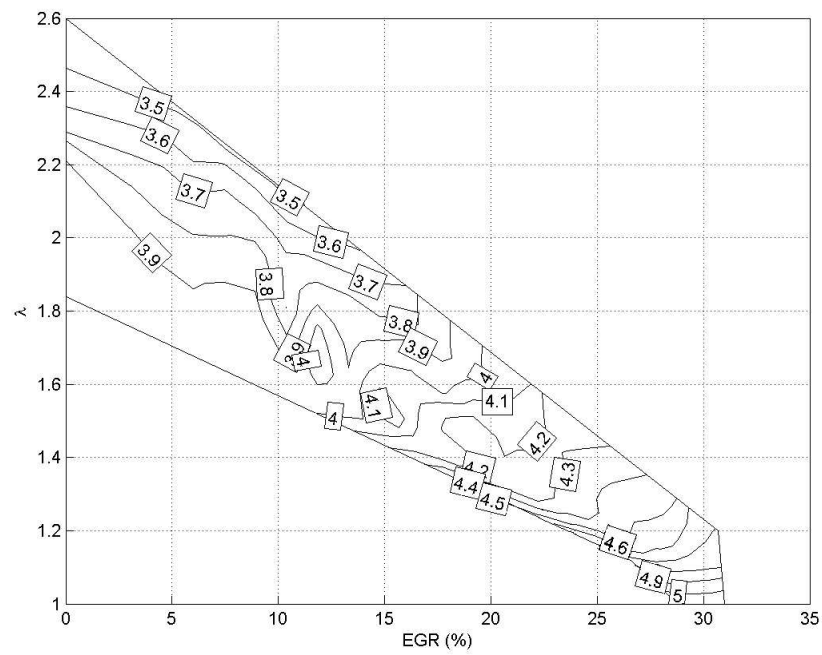
Figure 4.4: IMEP in bar for PRF20
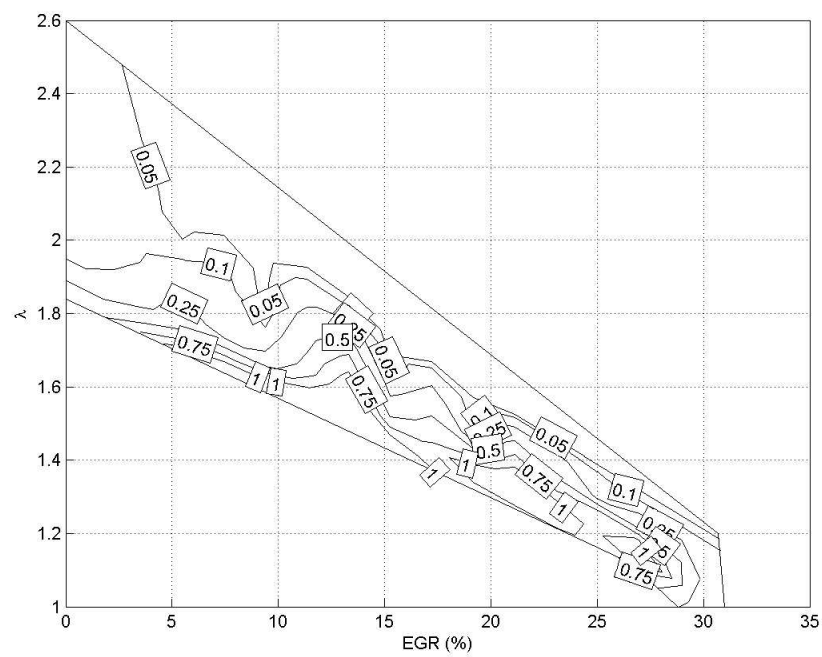
Figure 4.5: Indicated Specific NO$_x$ in g/kWhr for PRF20
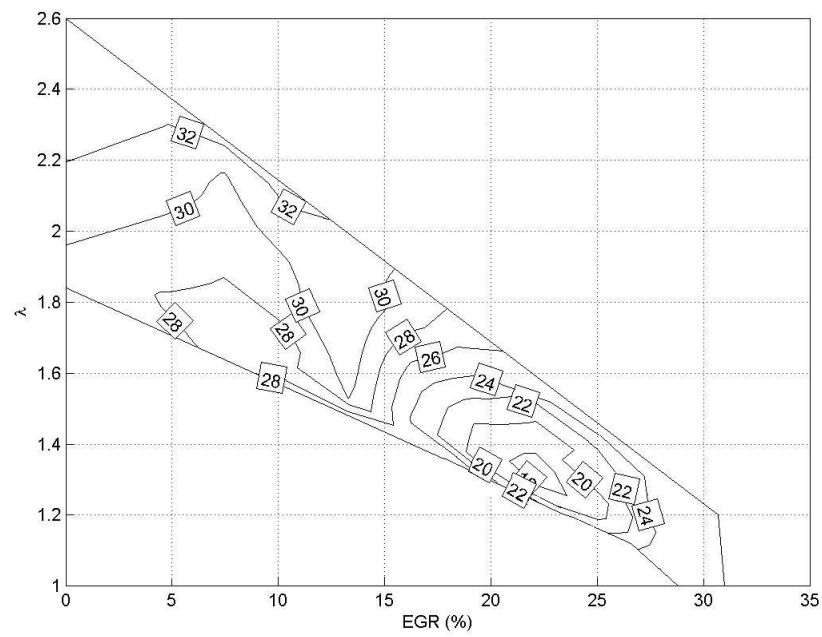
Figure 4.6: Indicated Specific HC in g/kWhr for PRF20
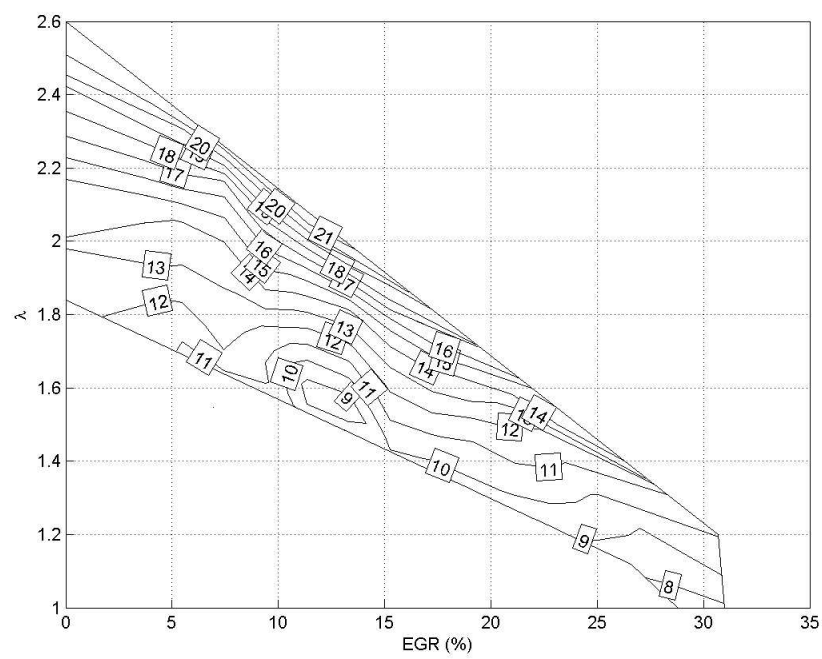
Figure 4.7: Indicated Specific CO in g/kWhr for PRF20
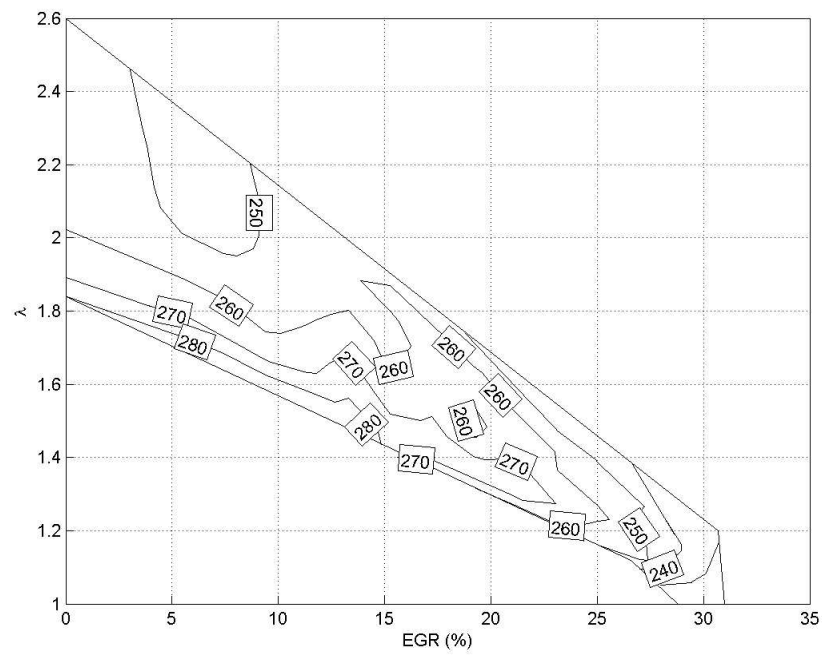
Figure 4.8: ISFC in g/kWhr for PRF20
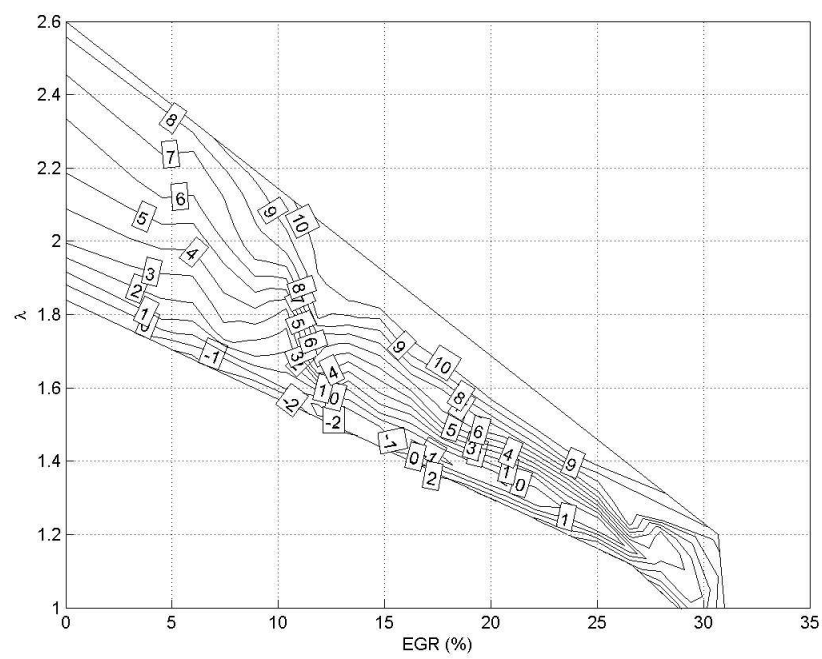
Figure 4.9: Start of Combustion (10% Burnt) in degrees for PRF20
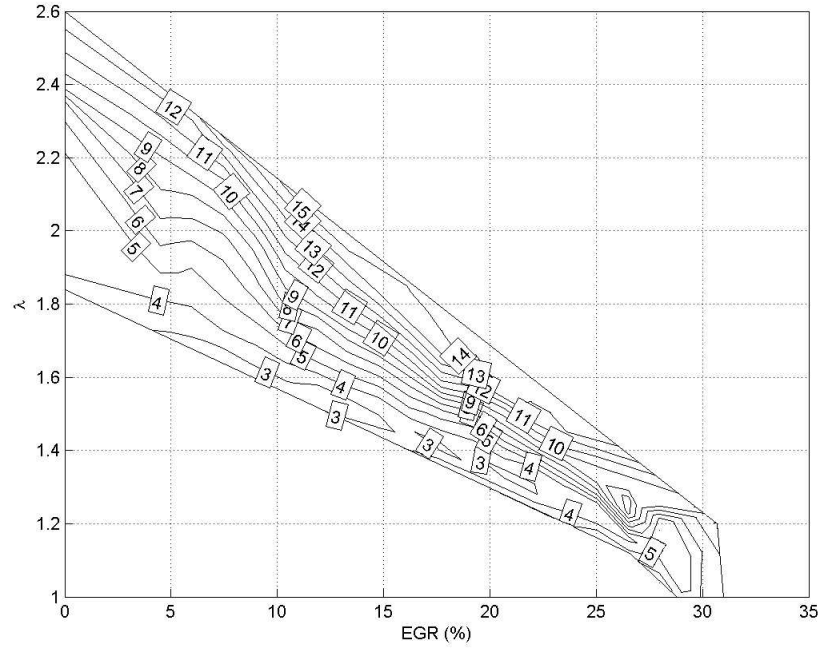
Figure 4.10: Burn Duration (10-90% Burnt) in degrees for PRF20

4.3 PRF40 and PRF60

The effect of ON on operating region, IMEP, indicated specific emissions, ISFC, SOC, and burn duration are examined by comparing two points from similar locations from each ON. Point A is selected at the minimum percent EGR and approximately the median λ at that percent EGR. Point B is selected at the maximum percent EGR and slightly above stoichiometric ($\lambda \approx 1.07$). Points A and B for the three fuels are shown in Figures 4.2, 4.11 and 4.20.

4.3.1 Operating Region

As the ON increases, the operating region size decreases (Figures 4.11 and 4.20). The effective dilution also decreases as the ON increases (Figures 4.12 and 4.21). This occurs because the auto-ignition process of HCCI is controlled by chemical kinetics [Najt and Foster, 1983]. The auto-ignition process occurs when the energy released by large

numbers of simultaneous interdependent chain reactions is larger than the heat lost to the surroundings. The rate that these chain reactions propagate is not the same for every fuel. For straight-chain paraffins (n-heptane) the rate of chain propagation is more intense than that of a branched chained paraffins (iso-octane) [Milovanovic and Chen, 2001]. Long chained fuels (n-heptane) have many weakly bonded H atoms and a high isomerization rate which lead to rapid ignition. For compact and highly branched fuels (iso-octane) with a large fraction of strongly bonded H atoms, isomerization and ignition is inhibited. As a result, less dilution is required to control the combustion rate as the ON is increases, thus reducing the operating region.

4.3.2 Indicated Mean Effective Pressure

IMEP for PRF40 and PRF60 are shown in Figures 4.13 and 4.22, respectively. The behavior that occurs near the knock boundary in the PRF20 case is magnified in both the PRF40 and PRF60 cases. The PRF40 case (Figure 4.13) shows the IMEP increase, as lambda is increased, between 0 and 17% EGR. Above 17% EGR, the IMEP becomes nearly independent of EGR and decreases as lambda is increased. The IMEP for PRF60 (Figure 4.22) shows the IMEP increase, as lambda is increased, between 0 and 9.5% EGR. Above 9.5% EGR the IMEP decreases as the lambda is increased.

As indicated before this behavior is due to the mild knocking which causes increased heat transfer to the piston and cylinder walls resulting in a slightly lower IMEP. The behavior does not occur at higher EGR levels because EGR is able to reduce heat transfer to the cylinder walls due to the increased specific heat capacity of EGR compared to excess air. The PRF40 and PRF60 cases magnify this IMEP behavior because the audible mild knock region during testing became larger as the ON is increased.

To understand the effect of EGR and excess air dilution on IMEP, Points A and

B for the three different ON, are compared in Table 4.3. The IMEP at Point B is consistently higher than the IMEP at Point A because the dilution is lower at Point B. Generally, the IMEP increases as the ON increases. This occurs because increasing the ON requires less dilution for stable HCCI combustion, as a result there is more chemical energy in the mixture and the IMEP increases.

4.3.3 Indicated Specific Emissions

Oxides of Nitrogen Emissions

The NO_x emissions for the PRF40 (Figure 4.14) and PRF60 (Figure 4.23) exhibit similar trends to the PRF20 (Figure 4.5). NO_x emissions are highest near the knock boundary and are lowest near at the misfire boundary. The iso-lines are nearly parallel to the knock and misfire boundaries. This indicates that the NO_x decreases as the dilution increases with either excess air or EGR.

For the majority of the map, the NO_x emissions for PRF40 and PRF60 are more sensitive to small changes in excess air than small changes in EGR. However, near stoichiometric, the iso-lines become vertical and curve clockwise into the knock boundary. This indicates that NO_x is more sensitive to EGR, than lambda. This effect also becomes more apparent with increasing ON. As discussed previously, this occurs because the increased oxygen concentration offsets the reduction in combustion temperature in the formation of NO_x. All three fuels exhibit a localized peak in NO_x emissions about $\lambda = 1.11$.

For the Points A and B the overall NO_x magnitude increases as the ON increases (Table 4.3). This occurs because the dilution is decreasing and load is increasing which results in higher combustion temperatures. The increase in NO_x from the PRF40 to PRF60 case indicates that the reduced dilution in the PRF60 case causes increased combustion temperatures, in some cases above 1800K where the NO_x for-

mation becomes significant.

Table 4.3: Point A and B Comparison / IMEP, Emissions and ISFC

	IMEP (bar)	NO$_x$ (g/kWhr)	HC (g/kWhr)	CO (g/kWhr)	ISFC (g/kWhr)
PRF20					
Point A	3.88	0.04	33.0	14.1	247
Point B	4.85	0.62	20.6	7.6	224
PRF40					
Point A	4.40	2.22	28.5	10.6	270
Point B	5.31	1.17	21.3	4.9	241
PRF60					
Point A	4.78	6.61	49.5	13.2	285
Point B	5.73	4.68	22.3	4.7	265

Unburn Hydrocarbons Emissions

Figures 4.15 and 4.24 shows the unburned hydrocarbon emissions for PRF40 and PRF60, respectively. The PRF40 exhibits similar trends to PRF20. Generally, the HC are a minimum near the knock boundary, where the combustion temperature are the highest, and are a maximum near the misfire boundary. The HC emissions are also slightly lower near stoichiometric condition than at zero percent EGR.

The HC emissions for PRF60 case are slightly different than HC emissions for the PRF20 and PRF40 cases. The HC emissions are highest near the knock boundary and are lowest near the misfire boundary, which is opposite to the PRF20 and PRF40 cases. The PRF60 exhibited higher knock levels compared to the other fuels. Higher knock levels have substantial variations in the combustion from cycle-to-cycle [Nakagawa et al., 1983]. Thus, the high HC emissions near the knock boundary are a result of poor combustion cycles.

Table 4.3 compares the HC emissions for the three fuels at Points A and B. The HC emissions stay roughly constant and do not decrease as the ON is increased (except

for Point A of PRF60). This occurs because the knock level increases with increased ON due to reduced dilution, causing higher cycle-to-cycle variation in combustion. This results in higher HC emissions. Any reduction in HC emissions due to increased combustion temperature (reduced dilution) is offset by the higher cycle-to-cycle variation in the combustion. Thus, the HC emissions remain relatively constant between the three fuels.

Carbon Monoxide Emissions

The CO emissions for the PRF40 (Figure 4.16) case exhibit similar trends to the PRF20 case. The CO emissions in PRF40 are lower near the knock boundary, where the combustion temperature are the highest, and are highest near the misfire boundary. The CO emissions are also lower near stoichiometric condition where the dilution is at a minimum, than at low EGR conditions.

The PRF60 case (Figure 4.25) is slightly different from PRF20 and PRF40. From 8 to 16% EGR, the CO emissions are higher near the knock boundary, than near the misfire boundary. This is similar to the HC emissions for the PRF60 case and is likely due to the higher cycle-to-cycle variation near the knock boundary. From 0 to 8% the CO emissions are lower at the knock boundary and decreases as λ is increased.

Table 4.3 shows that the CO emissions decrease between PRF20 and PRF40. This occurs because the PRF40 case has less dilution compared to the PRF20, thus the combustion temperatures are higher and more of the CO is oxidized to CO_2. Point B of the PRF60 case also decreased, although only slightly from Point B of the PRF40 case. Point A of the PRF60 case increased from Point A of the PRF40 case. Thus, the CO emissions for PRF60 case are generally higher due to the cycle-to-cycle variation in the combustion, similar to the HC emissions.

4.3.4 Indicated Specific Fuel Consumption

The ISFC map for PRF40 and PRF60 are presented in Figures 4.17 and 4.26, respectively. Both ISFC trends are similar to the PRF20. ISFC decreases as the mixture became more diluted, either with excess air or EGR. The minimum ISFC occurs near stoichiometric condition and the maximum ISFC occurs along the upper half of the misfire boundary. The minimum ISFC occurs near stoichiometric due to reduced pumping losses.

Comparing the three Point A's and the three Point B's in Table 4.3, ISFC increases with increased ON. This occurs because dilution is decreasing as the ON is increasing. Lower dilution means higher combustion temperatures which results in more heat loss to the cylinder walls and less of the fuel's energy being transferred as work to the piston.

4.3.5 Start of Combustion and Burn Durations

Figures 4.18 and 4.27 show the SOC maps for the PRF40 and PRF60, respectively. The PRF40 exhibits similar trends to the PRF20 case. The SOC iso-lines are nearly parallel with the knock and misfire boundaries and the SOC increases as the dilution increases. Also, the SOC is more sensitive to small increases in lambda, than small increases in EGR, particularly near stoichiometric. The PRF60 case exhibits iso-lines parallel to the boundaries from 0 to 9% EGR. However, from 9 to 16% EGR, the iso-lines became nearly vertical, indicating the SOC becomes more sensitive to small changes in EGR, than lambda in this region.

Table 4.4 shows that the SOC occurs later as ON is increased, except for Point A of PRF40. The rate of chain propagation for straight-chain paraffins (n-heptane) is more intense than that of a branched chained paraffins (iso-octane). Long chained fuels (n-heptane) have many weakly bonded H atoms and a high isomerization rate,

which leads to rapid ignition. For compact and highly branched fuels (iso-octane) with a large fraction of strongly bonded H atoms, ignition is inhibited. As the ON is increased the ignition is further inhibited by the iso-octane and requires more time to reach the proper conditions to auto-ignite.

Table 4.4: Point A and B Comparison / ERG, λ, SOC, Burn Duration and Dilution

	EGR (%)	λ	SOC (after TDC) (deg)	Burn Duration (deg)	Effective Dilution
PRF20					
Point A	1.8	2.10	4.2	6.2	1.06
Point B	29.8	1.07	4.5	4.0	0.47
PRF40					
Point A	1.3	1.64	2.4	5.5	0.62
Point B	23.8	1.08	10.0	5.6	0.38
PRF60					
Point A	1.3	1.49	7.7	3.9	0.48
Point B	15.2	1.08	15.4	7.3	0.25

The burn duration map for PRF40 and PRF60 is presented in Figures 4.19 and 4.28, respectively. The PRF40 exhibits similar trends to the PRF20 case. The iso-lines are nearly parallel with the knock and misfire boundaries and the burn duration increases as the dilution increases. Also, the burn duration for the PRF40 is more sensitive to increases in lambda, than EGR. The PRF60 case exhibits iso-lines parallel to the boundaries from 0 to 9% EGR, however, from 9 to 16% EGR, the iso-lines became nearly vertical. This indicates the burn duration is more sensitive to increases in EGR, than lambda.

For Point A the burn duration decreases with ON since EGR is nearly constant and λ is decreasing (Table 4.4). For Point B the EGR level is decreasing as ON increases resulting in the burn duration increasing. This indicates that the burn duration is not significantly affected by the ON, but predominately influenced by the EGR and λ.

4.3.6 Figures - PRF40
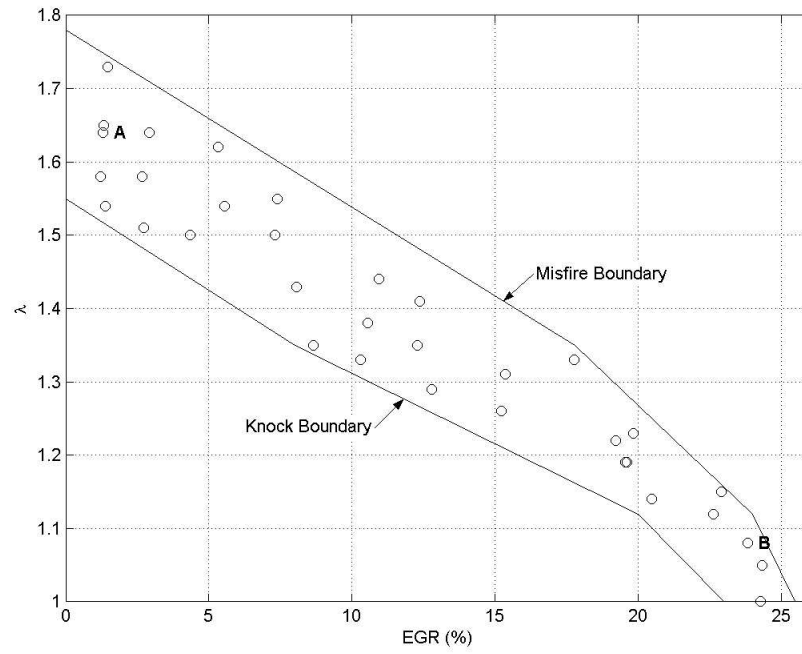
Figure 4.11: HCCI Operating Region for PRF40
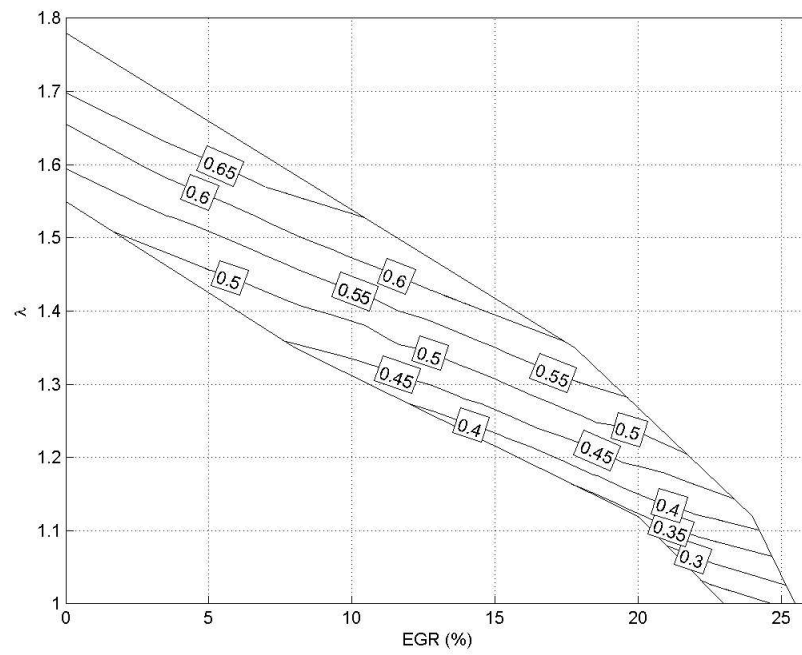
Figure 4.12: Effective Dilution for PRF40
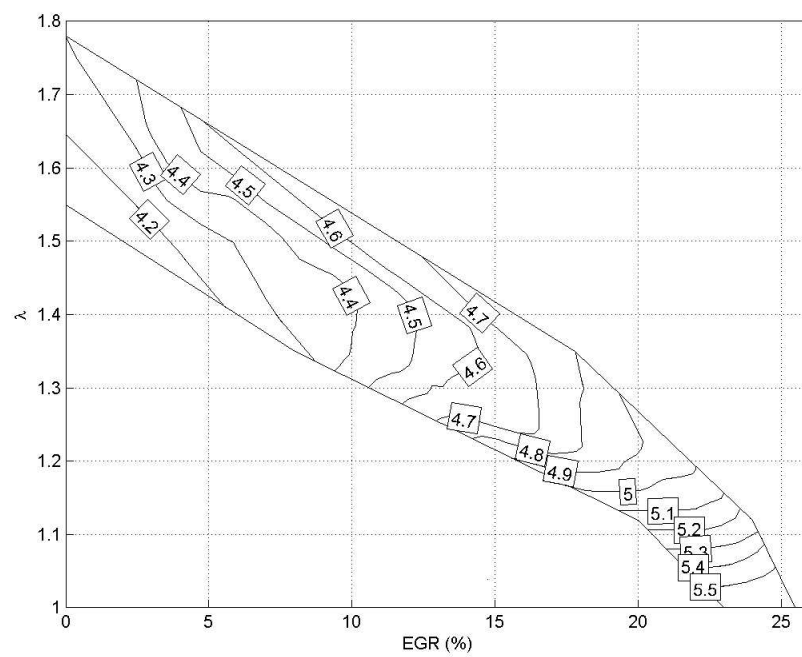
Figure 4.13: IMEP in bar for PRF40
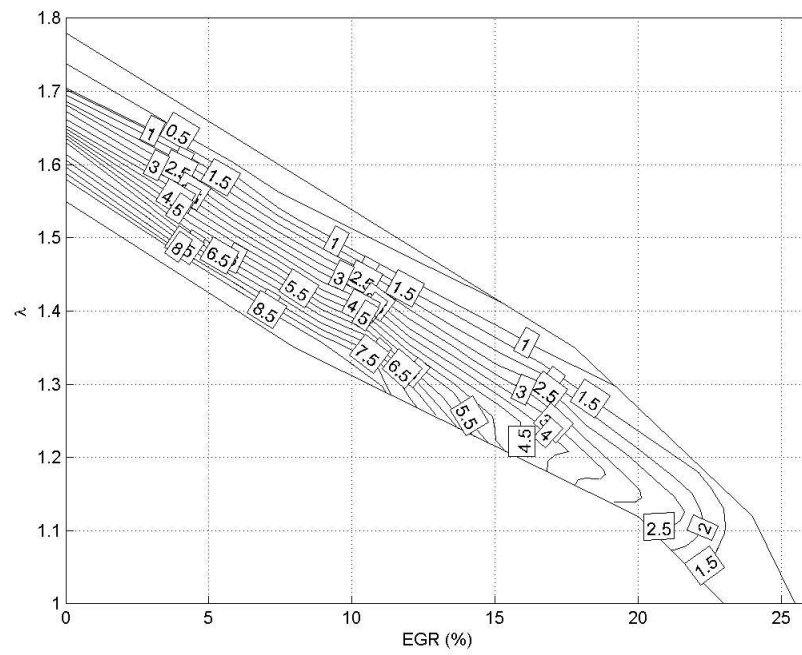
Figure 4.14: Indicated Specific NO$_x$ in g/kWhr for PRF40
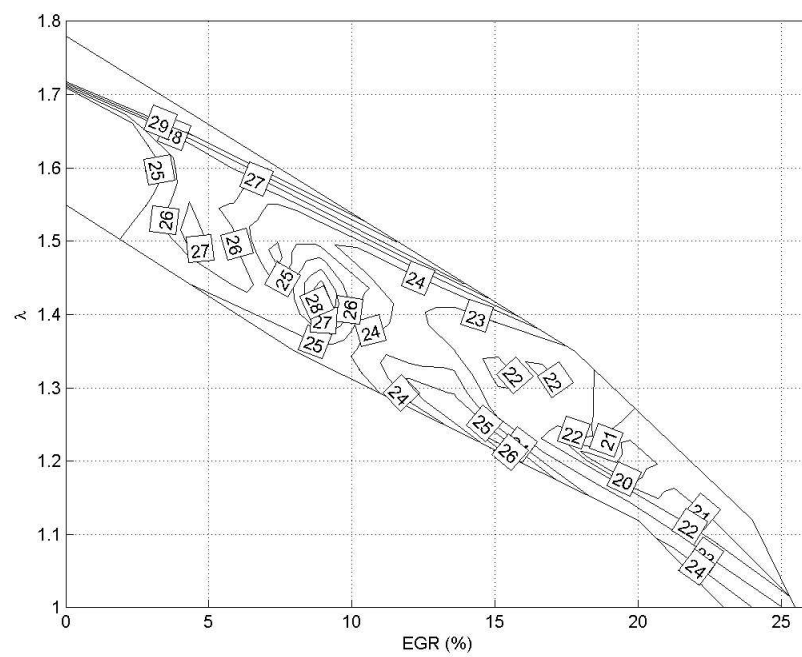
Figure 4.15: Indicated Specific HC in g/kWhr for PRF40
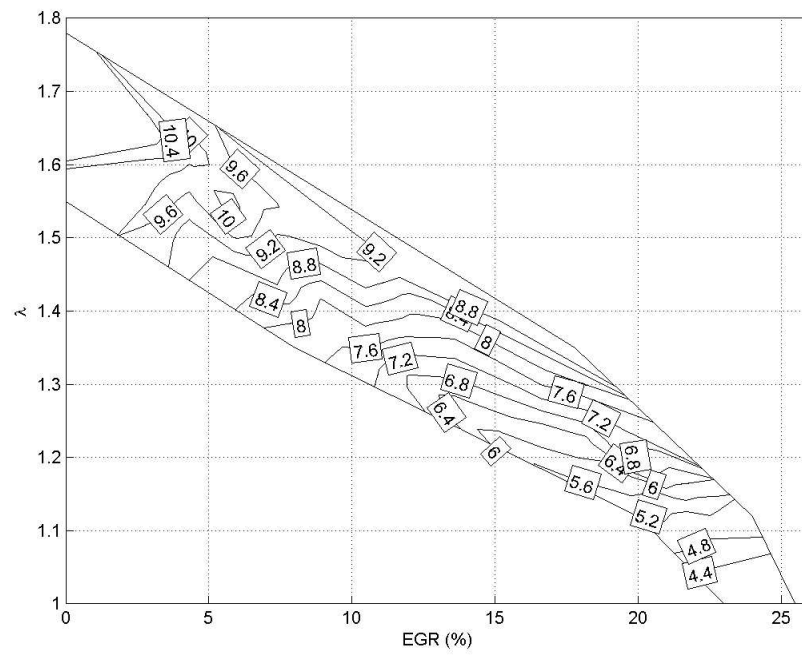
Figure 4.16: Indicated Specific CO in g/kWhr for PRF40
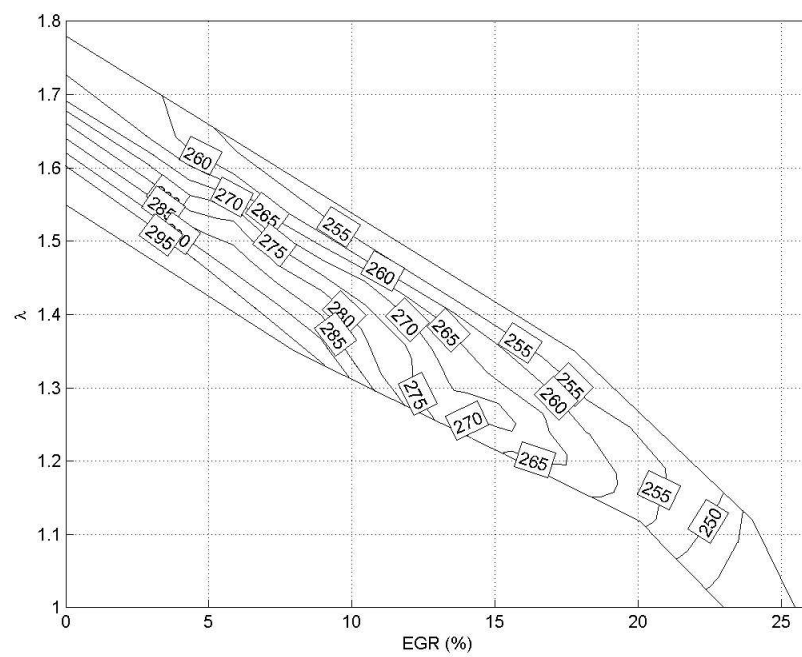
Figure 4.17: ISFC in g/kWhr for PRF40
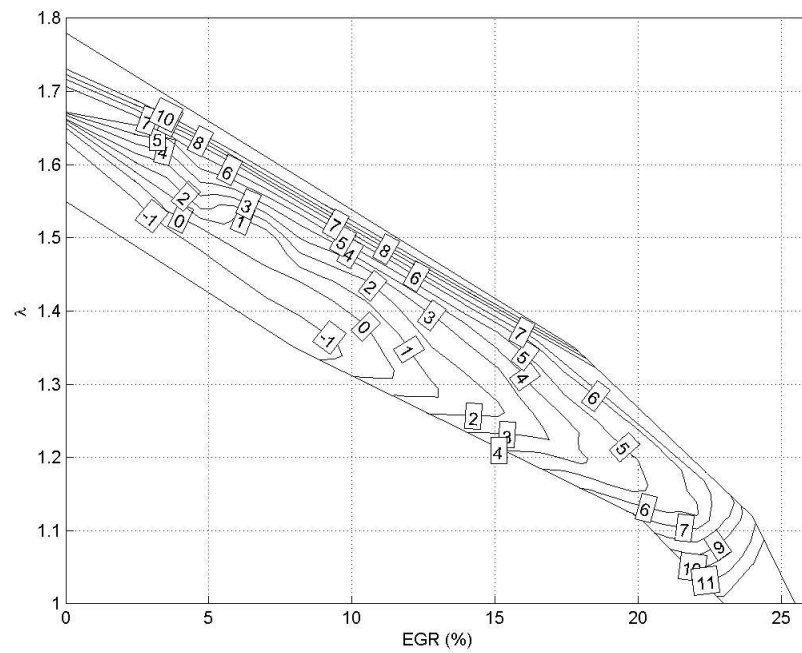
Figure 4.18: Start of Combustion (10% Burnt) in degrees for PRF40
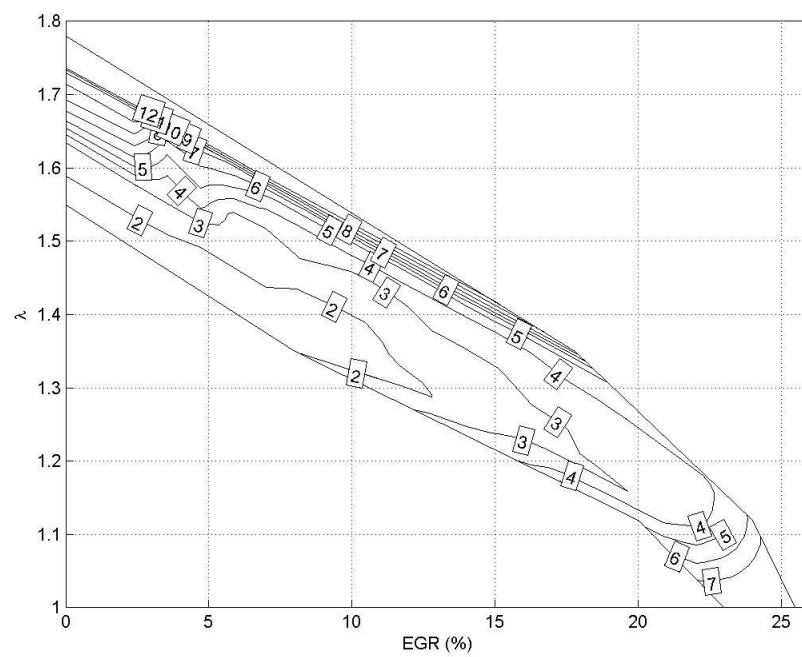
Figure 4.19: Burn Duration (10-90% Burnt) in degrees for PRF40

4.3.7 Figures - PRF60
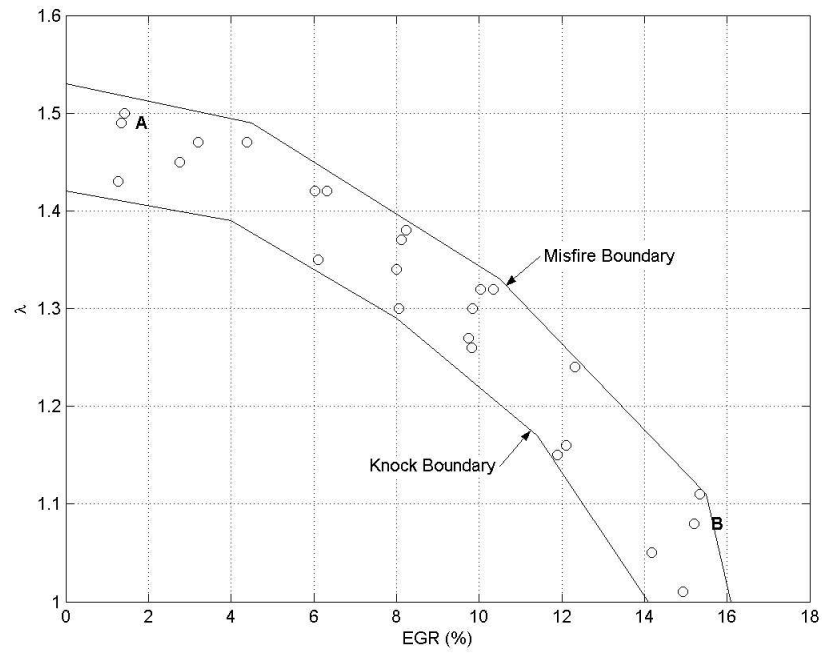
Figure 4.20: HCCI Operating Region for PRF60
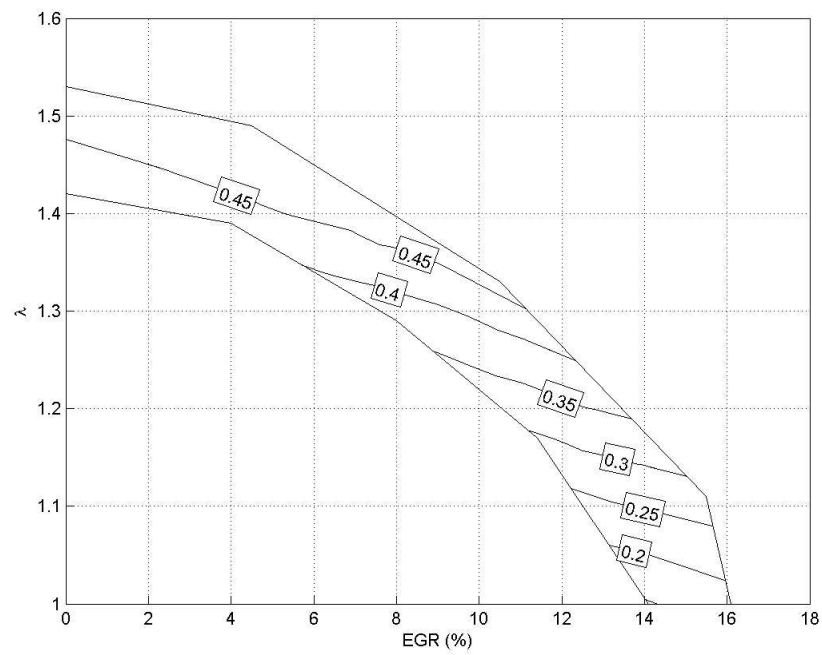
Figure 4.21: Effective Dilution for PRF60
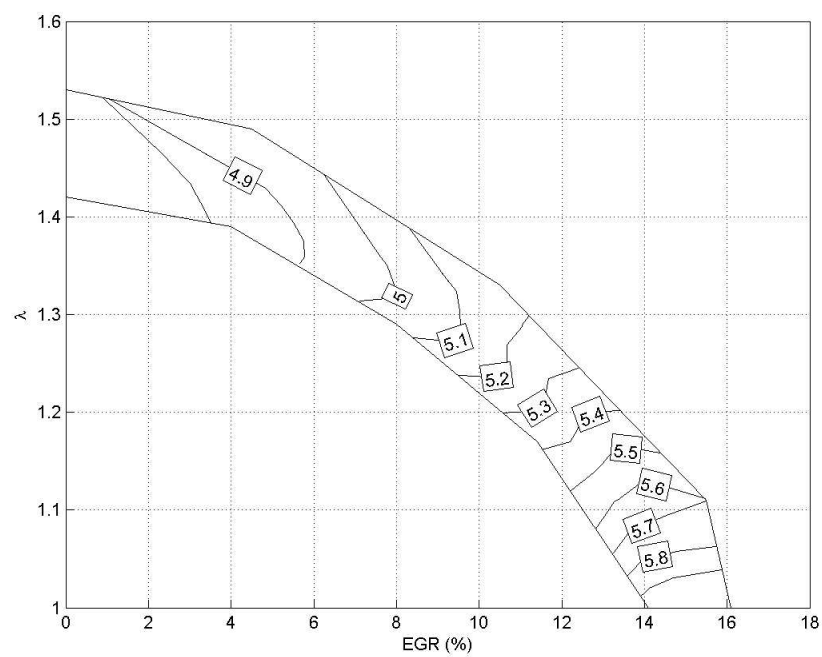
Figure 4.22: IMEP in bar for PRF60
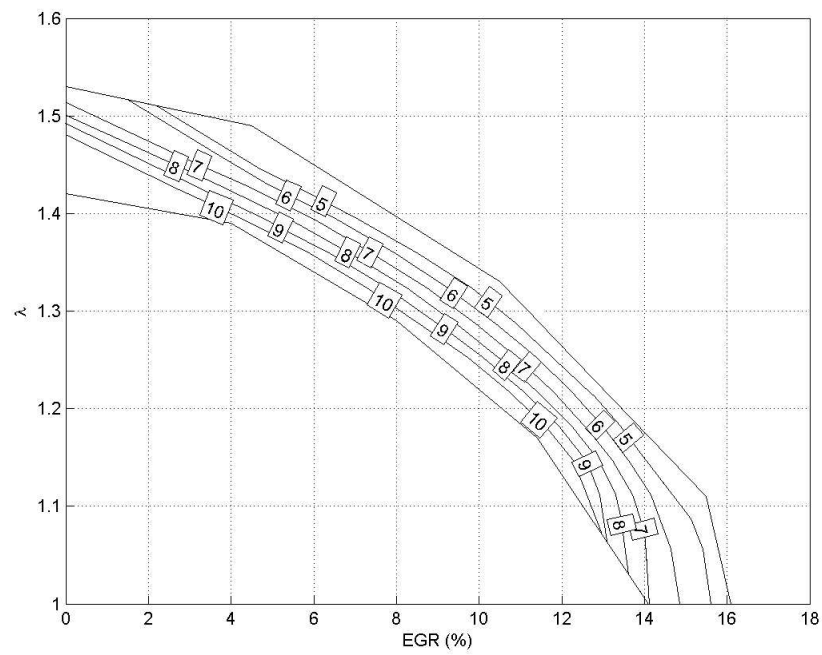
Figure 4.23: Indicated Specific NO$_x$ in g/kWhr for PRF60
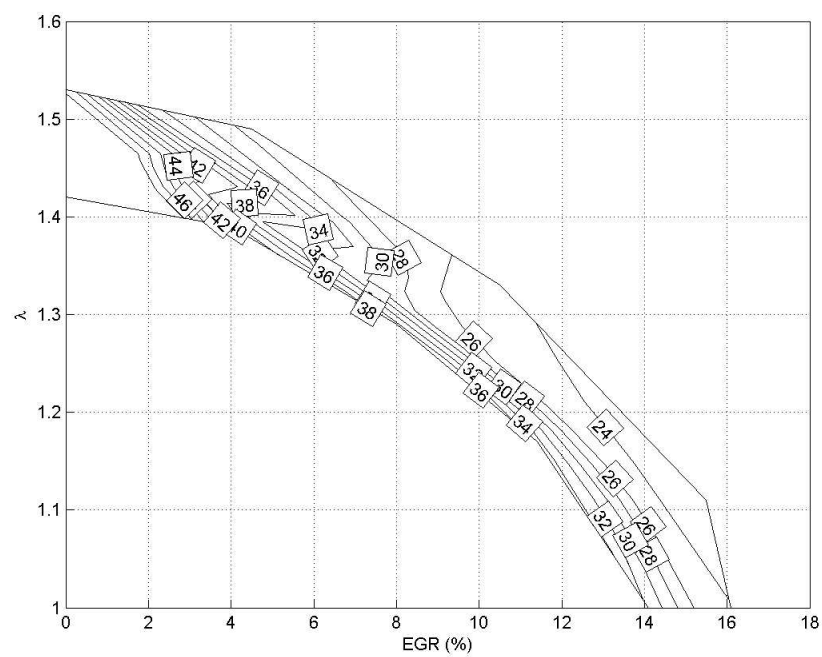
Figure 4.24: Indicated Specific HC in g/kWhr for PRF60
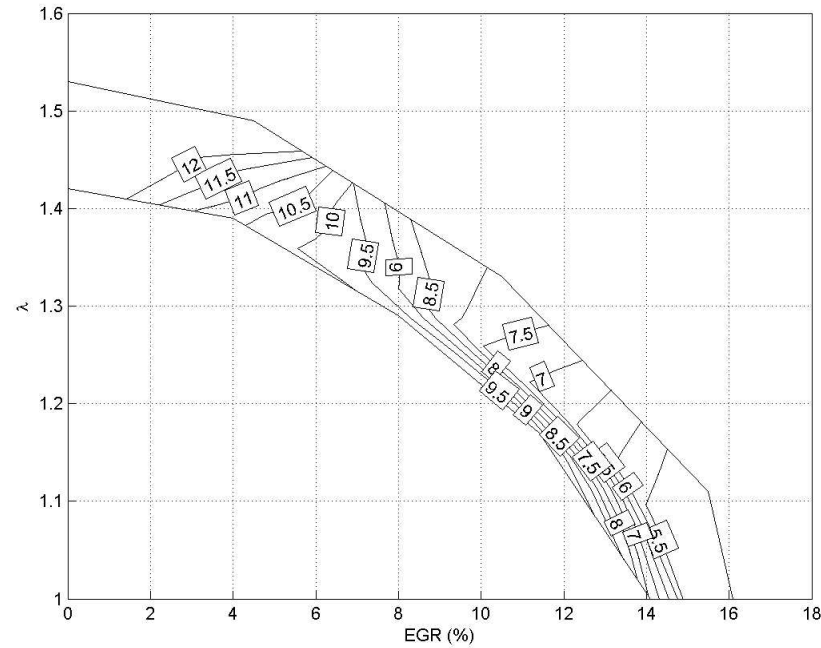
Figure 4.25: Indicated Specific CO in g/kWhr for PRF60
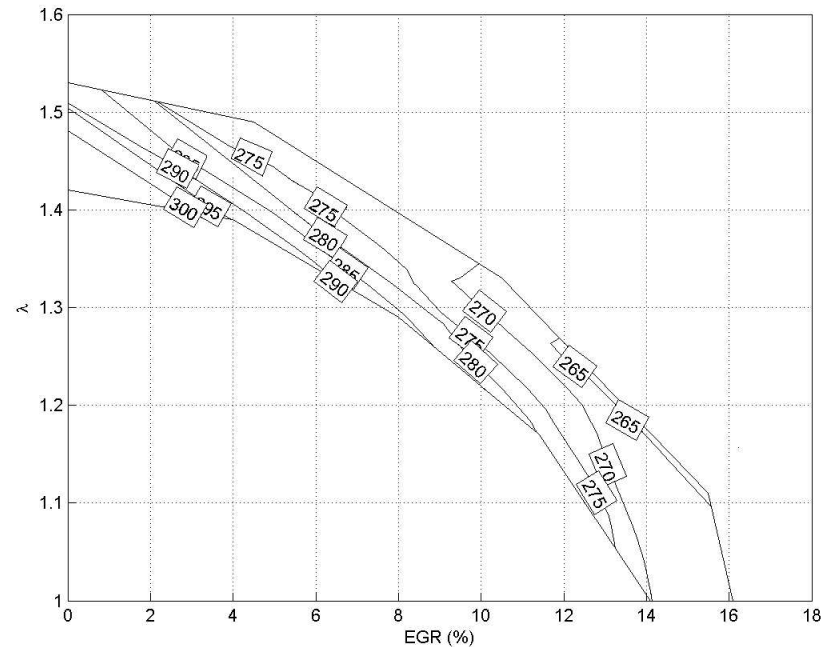
Figure 4.26: ISFC in g/kWhr for PRF60
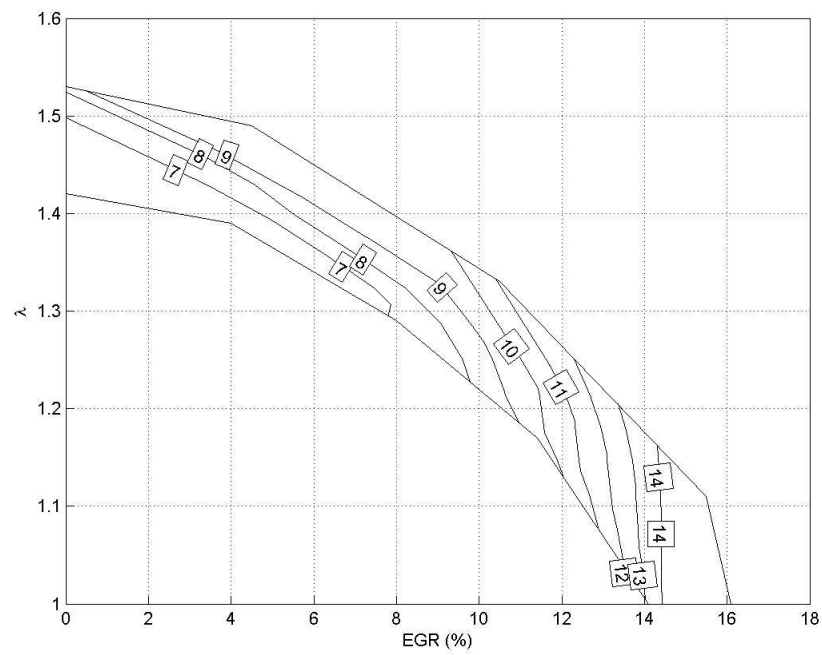
Figure 4.27: Start of Combustion (10% Burnt) in degrees for PRF60
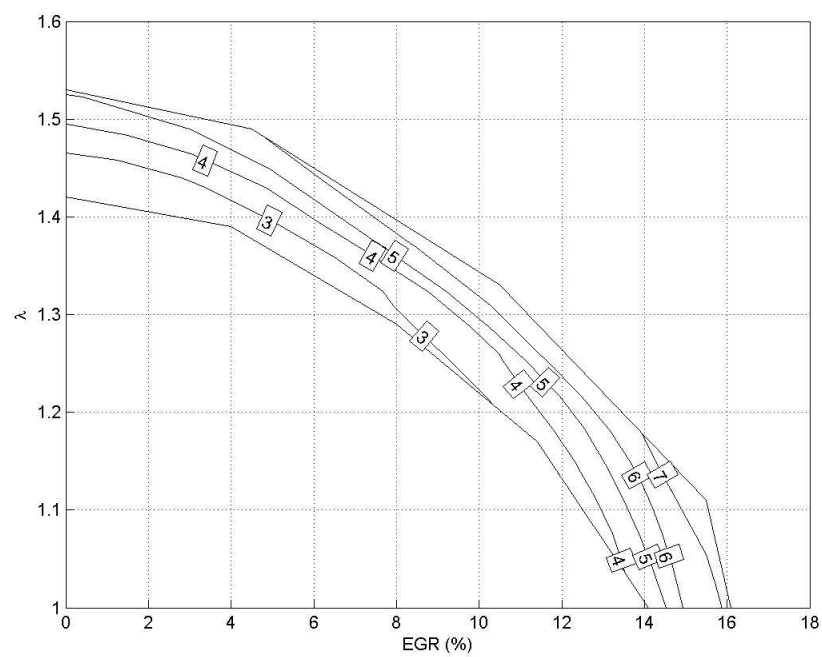
Figure 4.28: Burn Duration (10-90% Burnt) in degrees for PRF60

CHAPTER 5

DISCUSSION

The experiments conducted on a single cylinder research engine show that octane number, EGR, λ all influence HCCI combustion. A further discussion of these effects is outlined in this chapter.

5.1 Effects of Octane Number

The operating region as a function of EGR and λ of each of the three octane numbers is shown in Figure 5.1. The operating region for each ON is distinct from the others and the each higher ON fits under the next lower ON. The engine load range inside the operating regions is limited to $3.4 <$ IMEP < 5.9bar for all three fuels. The minimum load is too high for idling while the maximum load is too low for maximum power output. Two methods to further decrease the minimum load are increasing the intake air temperature or the compression ratio. This causes a higher mixture temperature which requires more dilution to control the combustion rate, resulting in lower IMEP. A method to extend the maximum IMEP is supercharging. This increases the total energy of the air/fuel in each engine cycle, resulting in increased IMEP.

IMEP generally decreases as the ON decreases, although IMEP overlaps between the different octane numbers. The lowest IMEP occurred with the PRF20 and the
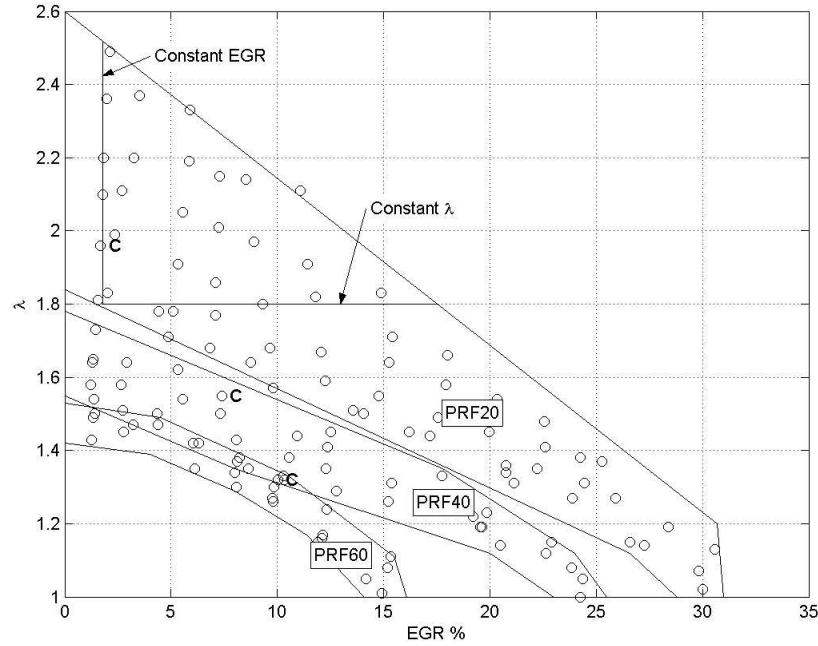
Figure 5.1: Operating Region For PRF20, PRF40 and PRF60

highest IMEP with the PRF60. Despite the lowest IMEP, the PRF20 generally has the best ISFC because PRF20 has the highest dilution which results in more work transferred to the piston, less heat loss to the cylinder walls and reduced pumping losses. If it is possible to control ON, then a control strategy that minimizes the ON in order to obtain the required engine load at the maximum possible dilution would minimize ISFC. However since ISFC does not continue to decrease as λ increases but reaches a minimum ISFC point lean of stoichiometric, the maximum dilution should not exceed the ISFC minimum. This minimum ISFC, which is strongly dependent on the combustion chamber design [Heywood, 1988], has not been found for this engine.

Figures 4.9, 4.18 and 4.27 show that the SOC does not significantly change with ON, but is very dependent on the mixture dilution. In addition, the burn duration is not significantly affected by the ON, but is predominately influenced by the mixture dilution. This shows that the ON is not an effective tool for changing the SOC or

burn duration but the ON is effective at increasing the load range.

A common method of increasing the efficiency of the traditional SI engine is by rasing the compression ratio. However, this requires the uses of high octane fuels in order to avoid knock related problems and can also result in higher NO_x emission levels. The increase in efficiency can also be offset by the cost increase associated with the higher octane fuels. This study shows that HCCI combustion results in a high efficient engine with very low NO_x emissions using a low octane (PRF20), poor quality fuel.

5.2 Effects of Dilution

In order to separate the individual effects of excess air and EGR, the effective dilution is examined along lines of constant EGR and constant lambda. The lines of constant EGR and constant lambda for the PRF20 are shown in Figure 5.1. The data points for the line of constant lambda have an average lambda of 1.80 and EGR increases from 1.6 to 14.9%. The data points for the line of constant EGR have an average EGR of 1.8% and lambda increases from 1.81 to 2.49.

The SOC and burn duration for constant EGR and constant λ, as a function of effective dilution (Equation 4.1) are shown in Figure 5.2. The SOC and the burn duration lengthens with increasing diluent which is in agreement with other experimental studies [Oakley et al., 2001, Peng et al., 2003]. Comparing the burn duration at fixed λ and fixed EGR, the EGR is shown to be a more effective diluent in slowing down the combustion (Figure 5.2). SOC is also later for a given amount of EGR diluent compared to air (λ) as a diluent. Combustion simulation in Zhao et al. [2002] indicates that the SOC is predominately affected by the thermal effect of EGR while the burn duration is mostly affected by the thermal and dilution effects of EGR, which is consistent with these experimental results.
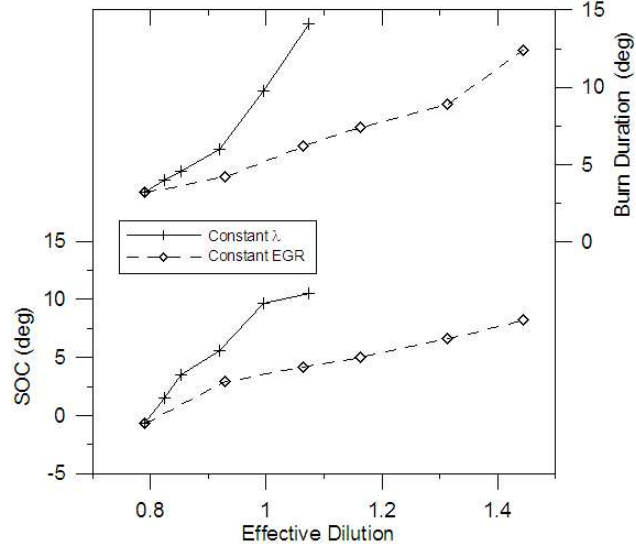
Figure 5.2: Start of Combustion and Burn Duration versus Constant EGR and Constant λ in degrees for PRF20 $\left(r_{Eff} = \frac{m_{EGR} + m_{Excess\ Air}}{m_{Stoichiometric}}\right)$

5.3 Oxides of Nitrogen, Octane Number and Peak Cylinder Pressure Correlation

A correlation between the indicated specific NO_x and peak cylinder pressure for each of the three ON is shown Figure 5.3. A parametric model of the form: $iNO_x = b_i + m_i e^{(\beta_1 \bar{P}^2 + \beta_2 \bar{P} + \beta_3)}$ where $\bar{P} = \frac{P}{P_0}$, P is the cylinder peak pressure, P_0 is a reference pressure, the parameters β_i are for the three fuel octanes and the coefficients b_i and m_i are for each individual octane number. The values of the coefficients and parameters are given in Table 5.1 and are obtained using a non-linear regression.

Table 5.1: NO_x versus Peak Pressure Correlation

Octane Number	m_i	b_i	β_1	β_2	β_3
ON 20	-0.284	0.960			
ON 40	-0.852	2.88	6.35	-8.84	1.34
ON 60	0.910	5.48			

Figure 5.1 shows the peak pressure versus the indicated specific NO_x emission with both the experimentally measured data points and the three regression lines for
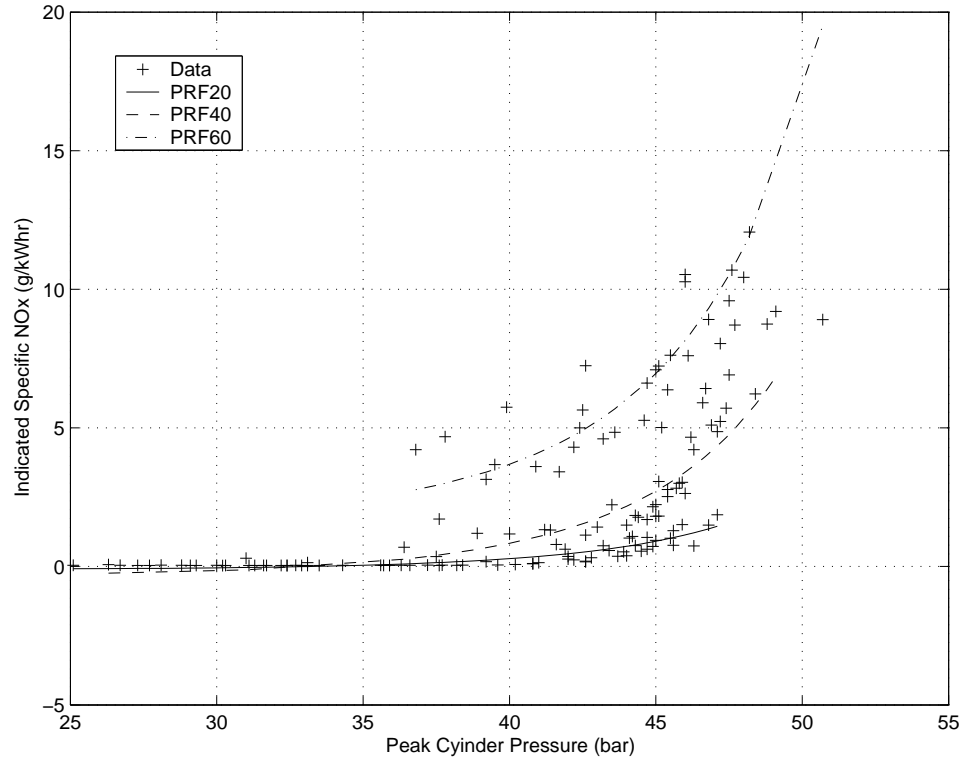
Figure 5.3: NO$_x$ versus Peak Pressure Correlation

each ON. As expected increasing the peak pressure increases the NO$_x$ emission levels for all the three fuels. Figure 5.3 shows that increasing the ON significantly increases the NO$_x$ emissions level even at the same peak pressure. This needs an explanation since peak temperature (and NO$_x$ formation) is normally directly correlated to peak pressure. The NO$_x$ emissions can be justified by referring to Table 5.2 in which

Table 5.2: Point C / NO$_x$ versus Peak Pressure Correlation

Fuel	EGR (%)	λ	IMEP (bar)	ISFC (g/kWhr)	NO$_x$ (g/kWhr)
PRF20	1.68	1.96	3.97	260	0.091
PRF40	7.39	1.55	4.53	259	0.62
PRF60	10.0	1.32	5.13	269	3.60

Fuel	HC (g/kWhr)	CO (g/kWhr)	SOC (deg)	Burn Duration (deg)	Peak Pressure (bar)
PRF20	34.6	13.3	2.9	4.2	40.8
PRF40	24.6	9.7	5.0	4.5	41.9
PRF60	24.9	7.9	11.3	5.5	40.9

the different parameters for the three different fuels at approximately the same peak pressure are tabulated (these points are indicated as Point C in Figure 5.1). For the three Point C's having the same peak pressure, the burn duration lengthens as the ON is increasing due to increased dilution. The longer burn duration means that the mixture is at elevated temperatures for a longer period of time resulting in more NO_x being formed at the same combustion temperature. Table 5.2 does not show the combustion temperature since this is difficult to measure, but the combustion temperature and pressure are highly correlated.

CHAPTER 6

Conclusions and Further Research

In this section the main conclusions are presented and then potential methods on how
the results here can be applied to HCCI operation in a vehicle are described. Then
recommendations of future work and methods of improving the experimental setup
are discussed.

6.1   Conclusions

The main goal of this study is to determine the effects of ON on the SOC and the
burn duration, for use in controlling HCCI combustion. To do this, experiments on
a single-cylinder engine have been conducted in which the ON and the dilution rate
(excess air and EGR) are varied. This study also examines the effect of dilution on
SOC and burn duration and discusses a correlation between NO_x emissions, ON and
peak cylinder pressure. The main conclusions of this work are as follows.

1. The octane number is not an effective tool for changing the SOC or burn du-
   ration. However, the octane number can be used to increase the load range,
   although the load range is still limited compared to a normal SI engine.

2. The HCCI operating region, as a function of EGR and λ, decreases in size as
   the octane number increases because higher octane fuels require less dilution to

control the combustion rate.

3. The IMEP or engine load increases as the octane number increases because the air/fuel mixture is less diluted, thus the mixture energy is greater for each individual engine cycle.

4. Increasing the octane number results in higher ISFC because the combustion temperatures are higher with reduced dilution. This results in less work being transferred to the piston and more heat being lost to the cylinder walls.

5. The NO_x emissions increase as the octane number increases because the peak combustion temperatures increase with reduced dilution. Results also show that HCCI engines have very low NO_x emissions compared to a SI engine. This is due to the homogenous and diluted air/fuel mixture.

6. Increasing the octane number delays the SOC because the chemical structure of iso-octane resists ignition. However, the burn duration is nearly unaffected by the octane number. The mixture dilution (λ and EGR) is more effective at influencing the SOC and the burn duration than the octane number.

7. After examining the individual effects of excess air and EGR, it is found that for the same amount of effective dilution, EGR is better at delaying the SOC and increasing the burn duration than excess air.

8. A non-linear statistical correlation of NO_x emissions to the peak cylinder pressure for all three octane numbers shows similar functional dependence. The correlation indicates that at the same peak pressure, higher octane fuels have higher NO_x emissions because the burn duration is longer at higher octane numbers.

6.2   HCCI Applications

The HCCI load range is limited to compared to a normal SI or CI engine. However, by varying the ON, the load range could be expanded allowing a greater region where HCCI would be possible. The ON could potentially be used to control the engine output as required in real engine operation (Conclusions 1 and 3).

Normal engine operation in production vehicles requires that the engine load and speed change rapidly in response to the driver's commands. Therefore, HCCI operation must be able to respond to both load and speed transients. In addition, to obtain high load operation, HCCI combustion would have to be switched to SI or CI combustion. The smooth transition from SI or CI to HCCI involves transient operation and is potentially difficult to obtain due to fast transients in cylinder temperatures and mixture composition. The combination of mixture dilution and ON could be used for fast transients and mode switching (Conclusions 2 and 6). Both ON and mixture dilution can be changed at a much faster rate than other techniques such as intake air heating.

Since EGR is more effective at controlling the SOC, a method of controlling the EGR would be critical for HCCI control (Conclusions 6 and 7). Variable valve timing is one possible method that this could be achieved. In addition, variable valve timing could be used for transient responses and mode switching.

A control strategy that uses the lowest possible ON for the required load would achieve the highest possible dilution. This would maximize engine efficiency and minimize NO_x emissions (Conclusions 4, 5 and 8). Also, contrary to SI engine trends, the use of a poor quality fuel with low ON results in the better engine efficiencies.

6.3 Further Research

Improvements to the experimental apparatus as outlined in the Section 6.4 are recommended. This would allow increased intake air heating and experiments using the full octane number range (PRF0 to PRF100) could be completed. From this, the entire load range available, from ON 0 to 100 could be determined and analyzed. Also, the minimum ISFC could be determined for this engine by incrementally increasing the intake air heating. Increasing the intake air temperature would increases the amount of dilution required to control the rate of combustion. Thus, the more work would be transferred to the piston and less heat loss to the cylinder walls as the dilution is increased, until cycle-to-cycle pressure fluctuations and increased burn duration degrades the ISFC.

The air/fuel ratio (λ) and percent EGR are far more effective at influencing the SOC and burn duration of HCCI combustion than the fuel octane number. Therefore, further examination of the effects of air/fuel ratio (λ) and the percent EGR on controlling HCCI should be conducted. This could be done by experimentally examining the effects of dilution, however, more physical insight into HCCI combustion could be obtained by researching a HCCI chemical kinetic model and than validating the model with experimental results. This would provide insight into the development of an accurate and dependable method of controlling HCCI combustion.

HCCI is limited to part load operation and will likely have to be switched to SI or CI combustion for high load operation. The transition from SI/CI to HCCI involves transient operation and is potentially difficult to manage. Few studies on HCCI transient operation or switching between HCCI and SI/CI mode [Fuerhapter et al., 2004] have been performed due to the complexity of HCCI combustion. More experimental and simulation transient HCCI results are needed to further characterize HCCI transient operation and switching combustion modes. Once HCCI transient

operation is clearly understood, a control strategy that is able to switch from SI/CI to HCCI combustion can then be developed.

6.4 Experimental Setup

Three main improvements of the experimental setup are proposed. First, the intake air heater which is currently installed upstream of the throttle and intake manifold should be installed inside of the manifold. This would better utilize the intake air heater by transferring more heat to the intake air and less to the intake manifold. This could be done by installing a finned tubular heating element (Model – FTS-036475) from Omega inside the manifold.

The second improvement that could be made is to the engine control module. The ECM was originally designed to be used with gaseous fuel and has a minimum fuel pulse width of approximately 3ms. However, for liquid fuels, the minimum fuel pulse width is too coarse to make fine adjustments of the air/fuel ratio. This could be corrected by using a different ECM that has a smaller minimum fuel pulse width.

The third improvement could be made to the emission sampling system. In order to determine the percent EGR, the CO_2 in the intake manifold has to be measured. A single CO_2 analyzer is used, with a two way solenoid valve, which allows both the exhaust gas composition and intake manifold composition to be measured. The solenoid valve is switch manually which also switches the exhaust sample pump to the intake sample pump. This causes the pressure in the intake manifold to drop about $\approx 2.5\%$. As a result, more EGR is ingested into the intake manifold which changes the operating conditions slightly.

Bibliography

(2001). Homogeneous Charge Compression Ignition (HCCI) Technology. U.S. Department of Energy (DOE), Energy Efficiency and Renewable Energy, Office of Transportation Technologies.

Aceves, S. M., Flowers, D. L., Martinez-Frias, J., Smith, J. R., Dibble, R., Au, M., and Girard, J. (2001a). HCCI Combustion: Analysis and Experiments. *SAE*, 2001-01-2077.

Aceves, S. M., Flowers, D. L., Martinez-Frias, J., Smith, J. R., Westbrook, C. K., Pitz, W. J., Dibble, R., Wright, J. F., Akinyemi, W. C., and Hessel, R. P. (2001b). A Sequential Fluid-Mechanic Chemical-Kinetic Model of Propane HCCI Combustion. *SAE*, 2001-01-1027.

Aroonsrisopon, T., Sohm, V., Werner, P., Foster, D. E., Morikawa, T., and Iida, M. (2002). An Investigation Into the Effect of Fuel Composition on HCCI Combustion Characteristics. *SAE*, 2002-01-2830.

Brown, B. R. (2001). Combustion Data Acquisition and Analysis. Master's thesis, Loughborough University.

Christensen, M., Hultqvist, A., and Johansson, B. (1999). Demonstrating the Multi Fuel Capability of a Homogeneous Charge Compression Ignition Engine with Variable Compression Ratio. *SAE*, 1999-01-3679.

Christensen, M. and Johansson, B. (1998). Influence of Mixture Quality on Homogeneous Charge Compression Ignition. *SAE*, 982454.

Christensen, M. and Johansson, B. (2001). The Effect of Piston Topland Geometry on Emissions of Unburned Hydrocarbons from a Homogeneous Charge Compression Ignition (HCCI) Engine. *SAE*, 2001-01-1893.

Christensen, M., Johansson, B., and Einewall, P. (1997). Homogeneous Charge Compression Ignition (HCCI) using Iso-Octane, Ethanol and Natural Gas - A Comparison with Spark-Ignition Operation. *SAE*, 972874.

Dec, J. E. and Sjöberg, M. (2003). A Parametric Study of HCCI Combustion – The Sources of Emissions at Low Loads and the Effects of GDI Fuel Injection. *SAE*, 2003-01-0752.

Fuerhapter, A., Unger, E., Piock, W. F., and Fraidl, G. K. (2004). The New AVL CSI engine – HCCI Operation on a Multicylinder Gasoline Engine. *SAE*, 2004-01-0551.

Heywood, J. B. (1988). *Internal Combustion Engine Fundamentals.* McGraw-Hill.

Iida, M., Hayashi, M., Foster, D. E., and Martin, J. K. (2003). Characteristics of Homogeneous Charge Compression Ignition (HCCI) Engine Operation for Variations in Compression Ratio, Speed, and Intake Temperature While Using n-Butane as a Fuel. *ASME*, Vol. 125, April 2003.

Kelly-Zion, P. and Dec, E. (2000). A Computational Study of the Effects of Fuel-Type on Ignition Time in HCCI Engines. *28th International Combustion Symposium.*

Kirchen, P. N. (2004). Thermokinetic Modelling of the HCCI Cycle. Master's thesis, University of Alberta.

Law, D. and Allen, J. (2002). On the Mechanism of Controlled Controlled Auto Ignition. *SAE*, 2002-01-0421.

Milovanovic, N. and Chen, R. (2001). A Review of Experimental and Simulation Studies on Controlled Auto-Ignition Combustion. *SAE*, 2001-01-1890.

Najt, P. M. and Foster, D. E. (1983). Compression-Ignited Homogeneous Charge Combustion. *SAE*, 830264.

Nakagawa, Y., Takagi, Y., Itoh, T., and Iijima, T. (1983). Laser Shadowgraphic Analysis of Knocking in SI Engine. *SAE*, 845001.

Noguchi, M., Tanaka, Y., Tanaka, T., and Takeuchi, Y. (1979). A Study on Gasoline Engine Combustion by Observation of Intermediate Reactive Products during Combustion. *SAE*, 790840.

Oakley, A., Zhao, H., Ladommatos, N., and Ma, T. (2001). Experimental Studies on Controlled Auto-ignition (CAI) Combustion of Gasoline in a 4-Stroke Engine. *SAE*, 2001-01-1030.

Oppenheim, A. K. (1984). The Knock Syndrome - Its Cures and Its Victims. *SAE*, 841339.

Owen, K. and Coley, T. (1990). *Automotive Fuels Handbook*. SAE.

Peng, Z., Zhao, H., and Ladommatos, N. (2003). Effects of Air/Fuel Ratios and EGR Rates on HCCI Combustion of n-heptane, a Diesel Type Fuel. *SAE*, 2003-01-0747.

Puzinauskas, P. V. (1992). Examination of Methods Used to Characterize Engine Knock. *SAE*, 920808.

Rassweiler, G. M. and Withrow, L. (1938). Motion Pictures of Engine Flames Correlated with Pressure Cards. *SAE*, Vol. 42.

Silvis, W. M. (1997). An Algorithm for Calculating the Air/Fuel Ratio from Exhaust Emissions. *SAE*, 970514.

Stanglmaier, R. H. and Roberts, C. E. (1999). Homogeneous Charge Compression Ignition (HCCI): Benefits, Compromises, and Future Engine Applications. *SAE*, 1999-01-3682.

Zhao, H., Li, J., Ma, T., and Ladommatos, N. (2002). Performance and Analysis of a 4-Stroke Multi-Cylinder Gasoline Engine with CAI Combustion. *SAE*, 2002-01-0420.

Zhao, H., Peng, Z., and Ladommatos, N. (2001). Understanding of Controlled Auto-Ignition Combustion in a Four-Stroke Gasoline Engine. *IMechE*, Vol. 215 Part D.

Appendix A

Experimental Setup and Instrumentation

This chapter gives a description of the experimental setup and instrumentation used in the investigation of HCCI combustion. The engine setup and instrumentation is described in Section A.1. The emission equipment used to determine the exhaust gas composition and percent EGR is described in Section A.2. Data is collected by two separate data acquisitions system which are described in Section A.3. Lastly, a list of equipment used in this study is given in Section A.4.

A.1 Engine Setup and Instrumentation

The engine used for the experimental work is a modified single-cylinder Co-operative Fuels Research (CFR) engine. The CFR engine, is a single-cylinder, continuously variable compression engine, originally designed to determine knock properties of different fuels. As a result, the engine is very durable and well suited to testing HCCI. The details of the engine are given in Table A.1. The engine has a pancake combustion chamber, originally designed to minimize turbulence or swirl and induce engine knock. HCCI is not dependent on turbulence for flame propagation or swirl flow for diffusion combustion [Christensen and Johansson, 1998], thus the combustion chamber is suitable for HCCI combustion research.

The original intake manifold and carburetor are replaced with a larger volume

Table A.1: Engine Specifications

Engine Type	Waukesha Motor Co., ASTM-CFR Engine
Bore × Stroke	83mm × 114mm (3.25in × 4.5in)
Displacement	0.612L (37.3cu in)
Compression Ratio	12.0 to 1
Engine Cooling	Water Cooled

intake manifold that incorporates three fuel injectors near the intake port of the engine. The engine is setup with three injectors so that any combination of natural gas, hydrogen or gasoline can be used. The natural gas and hydrogen injectors are Bosch injectors and the gasoline injector is from a Ford 4.6L V8 engine. The injectors are operated by a modified Sparrow Engine Control Module (ECM) from Alternative Fuel Systems. The ECM is capable of injecting two different fuels simultaneously at various pulse widths. The fuel pulse width of each injector can be controlled by the operator on the fly with the SparroWatch program on a desktop PC. This allows the operator to control of the mass fuel rate and the mixture stoichiometry in the engine. The ECM requires a crank angle position signal and camshaft signal, in order to pulse the injectors at the correct injection timing. A 36 minus 1 tooth gear and a Ford proximity sensor are used to provide the crankshaft angular position. The 36 minus 1 tooth gear is mounted on crankshaft at the front of the engine. Camshaft position is provided by the stock CFR engine camshaft signal, used for spark timing. The camshaft signal uses an eddy current sensor and a single magnet mounted on the camshaft. The eddy current sensor pulses once per engine cycle.

The carburetor is replaced with a throttle body from a Suzuki Swift 1.0L engine, however, a restrictor plate with a 3/8 inch hole, is added between the throttle and the intake manifold, in order to achieve part throttle conditions. Although, all of the HCCI experiments are conducted at WOT. External EGR is routed into the intake manifold through a one inch diameter pipe, as shown in Figure A.1. The EGR line emerges right behind the exhaust port and enters the midpoint in the intake manifold.

This reduces any EGR cooling that can occur and ensures that the EGR is well mixed with the fresh charge. The EGR rate is controlled by adjusting a brass gate valve, located about midpoint in the EGR line.

Figure A.1: Engine Setup

A 2kW air heater from Omega is added upstream of the throttle body to heat the intake air. Additional heat is required in order to get the air/fuel mixture to auto-ignite. The mass air flow is measured with a Siemens hot wire anemometer. The mass air flow can also be measured with a stopwatch and a dry gas meter attached upstream of the air barrel. A 59L air barrel is attached upstream of the hot wire anemometer, in order to dampen the intake air pressure fluctuation caused by the engine.

The volume fuel flow is measured with a Max Machinery piston meter and transmitter. The transmitter outputs 115 pulse/cc, which is read by a Triad Industries fuel flow meter (Figure A.2). The fuel flow meter converts the pulses into a volume

fuel flow rate and also outputs a total volume consumed. A fuel pump and regulator from a Ford 4.6L engine are used to pressurize and regulate the liquid fuel system. The natural gas fuel rate is not measured, as natural gas is only used to warm up the engine to operating temperature.

Figure A.2: Instrumentation Setup

The intake manifold pressure and exhaust manifold pressure are measured with two Validynes pressure transducers. The intake manifold Validyne has a range of 0 to 10psi (vacuum), where as the exhaust manifold Validyne has a range of 0 to 20psi. An Erlenmeyer beaker with a rubber stop is placed in both the intake and exhaust pressure sample lines to eliminate any water that may travel through the pressure lines and dampen some of the larger pressure fluctuations.

The cylinder pressure is measured with a Kisler water-cooled ThermoCOMP pressure sensor. The Kisler transducer is a piezoelectric pressure transducer. The operating principle is that the pressure acts on a diaphragm, which transfers this force

to a quartz crystal. When the quartz crystal is put under load, the crystal produces an electrostatic charge that is proportional to the pressure change. An electrode transfers the charge to a charge amplifier, where it is integrated and converted into a positive voltage. This makes piezoelectric transducers very suitable for measuring rapid, dynamic pressure processes that occur in engines, however, they cannot be used for static pressures. The integration process also requires that the charge amplifier has to be reset periodically in order to avoid drift.

An optical encoder from BEI Industrial Encoders is connected to the crankshaft on the front of engine. The encoder provides 1/10 degree angular resolution. The encoder also produced one pulse per crankshaft revolution to provide a reference for each engine cycle.

The compression ratio is set to 12 to 1, although other compression ratios could have been explored. This is determined by setting the piston to TDC and then measuring the clearance volume by filling it with oil. The oil volume is dripped into the clearance volume through the spark plug hole on top of the cylinder head. The oil volume is measured precisely with a 100mL buret. Then the compression ratio can be determined by the using the engine stoke, bore and the clearance volume.

The intake air temperature is measured with a Copper/Copper-Nickel T-type thermocouple, mounted adjacent to the engine intake port (Figure A.3). The intake air temperature is controlled with a Programmable Temperature Controller. The Programmable Temperature Controller outputs a 4-20mA signal to a 208V / 25Amp Power Control that provides the appropriate power to the heater. This allow for closed loop control of the intake air temperature.

Kromel-Alumel K-type thermocouples are used to measure the exhaust gas temperature adjacent to the engine exhaust port, the EGR temperature prior to entering the intake manifold, the intake air temperature downstream of the heater and the exhaust gas sample temperature downstream of the cooling tower. The output from

Figure A.3: Temperature and Heater Instrumentation

the thermocouples is measured with an Omega temperature meter.

The CFR engine is connected to a Direct Current (DC) dynamometer. This consists of a DC motor/generator mounted on its trunnion bearings. A Digalog 1022A dynamometer controller is used to control the engine and dynamometer. The controller requires both a load signal and engine speed signal to operate. A load cell is attached to one side with counter weights on the other side (Figure A.2). Engine torque can be calculated by multiplying the load cell output by the moment arm from the centre of the dynamometer to the load cell (288mm / 11.3inch). Engine speed is obtained from a proximity sensor measuring the pulses from a 60 tooth gear mounted on the back of the dynamometer. The engine speed and load signals are also acquired by the data acquisition system. The dynamometer is capable of motoring the engine as well as absorbing power. The controller is capable of holding the engine speed constant or the engine load constant, however, all the tests are conducted at constant

engine speed.

A wide range air/fuel ratio analyzer from Engine Control and Monitoring is used to measure the air/fuel ratio without having to calculate the air/fuel ratio from the emission bench. The analyzer measures the air/fuel ratio using Universal Exhaust Gas Oxygen (UEGO) sensor. The UEGO sensor has a wide range (λ=0.4 to 10), fast response (<150ms) and is mounted directly in the engines exhaust. The electrochemical cell responds to O_2, CO, H_2, and HC in the exhaust to determine the air/fuel ratio (λ). The analyzer also has a programmable 0 to 5VDC analog output that is recorded by the data acquisition system.

A.2 Emission Apparatus

The exhaust gas composition is determined by using California Analytical Instruments emission analyzers. The emission bench includes, a paramagnetic oxygen (O_2) analyzer, a non-dispersive infrared carbon dioxide analyzer (CO_2) and carbon monoxide analyzer (CO), a flame ionization detector for total unburned hydrocarbon (HC), a heated flame ionization detector for unburned methane hydrocarbons (CH_4), and a chemiluminescence oxides of nitrogen analyzer (NO_x). The sample gas is filtered and cooled to remove any particulates and water from the sample gas prior to analyzing, in order to avoid incorrect readings and to avoid damaging the emission equipment. The instruments are calibrated with standard gases before each test. Table A.2 shows the range, accuracy and calibration value for each analyzer.

In order to determine the percent EGR in the reactants, the CO_2 concentration in the reactants has to be measured. A single CO_2 analyzer is used, with a two way solenoid valve, which allowed both the products composition and reactant composition to be measured. During testing, the emission bench is manually switched from the products CO_2 to the reactant CO_2 after 20 seconds has elapsed. This allows 115

Table A.2: Emission Equipment

Component	Model	Range	Accuracy	Calibration
O_2	100P	0-25%	10 ppm	0%, 4.2%, 10.5%, 16.8%, 21%
CO_2	300	0-20%	1% full scale	0%, 4.0%, 10.1%, 16.2%, 20.2%
CO	300	0-2.5%	1% full scale	0%, 0.49%, 1.23%, 1.96%, 2.45%
NO_x	300-CLD	0-3000 ppm	3 ppm	0, 402, 12066, 2011, 2815 ppm
CH_4	300-HFID	0-30000 ppm	0.1 ppm	0, 101, 503, 1006, 2515, 3521, 5030 ppm
HC	300-FID	0-30000 ppm	0.1 ppm	0, 101, 503, 1006, 2515, 3521, 5030 ppm

engine cycles to be recorded from the products, allows 20 seconds for the bench to reach steady state and allows 115 engine cycles to be recorded from the reactants.

A.3 Data Acquisition Systems

A real-time analysis program for basic engine parameters has been developed using MATLAB® xPC Target. xPC Target is a host-target solution for prototyping, testing, and deploying real-time systems using standard PC hardware. In xPC Target, a model is created on the host PC using Simulink® blocks, which is then compiled and linked into a relocatable executable image that is download to the target PC which is running a real-time operating system. After downloading the executable code, the model can be run and tested in real-time. This program is used because it uses readily available PC hardware and the data collected is already in MATLAB® binary file format which makes post-processing very convenient.

The target PC has two National Instrument PCI-MIO-16E-1 data acquisition boards. Each board has 8 differential analog inputs, 12 bit resolution, ±0.05 to ±10Volt analog input range and a 1.25MS/s maximum sampling rate. The signals that are acquired by the data acquisition boards are:

- engine speed and load – from the dynamometer controller

- intake and exhaust manifold pressure – from Validyne pressure transducers

- volume fuel rate – from the Triad Industries fuel flow meter

- mass air flow rate – from the hot wire anemometer

- air/fuel ratio – from the Engine Control and Monitoring fast air/fuel ratio analyzer

- percent O_2 – from the paramagnetic oxygen analyzer

- percent CO_2 and CO – from the non-dispersive infrared analyzer

- ppm HC – from the flame ionization detector

- ppm CH_4 – from the heated flame ionization detector

- ppm NO_x – from the chemiluminescence analyzer

All of the signals are sampled at 100Hz and data is recorded for 60 seconds at each HCCI operating point. The calibration equation from each signal is applied in the data acquisition program so that the data is in physical units, rather than voltages.

The calculated engine load from the dynamometer load cell is Brake Mean Effective Pressure (BMEP). In order to get IMEP, the engine friction is added to the BMEP. The engine friction or Friction Mean Effective Pressure (FMEP) is determined by motoring the engine at various speeds and measuring the required load. The CFR engine measured FMEP is 2.16bar at 700RPM, but since the engine is not firing during the friction test the loads on the piston and cylinders walls are slightly lower. Therefore, the calculated IMEP from the engine dynamometer is slightly low.

The cylinder pressure and crank angle position are measured by a MTS Combustion Analysis System (CAS). The CAS provides the ability to determine, in realtime,

combustion and engine operating parameters, including IMEP, maximum pressure rise, start of combustion, burn duration, and peak pressure. The cylinder pressure sampling rate is determined by the encoder resolution. The encoder used in this study has a resolution of 1/10 degree. Thus, the cylinder pressure is sampled every 1/10 degree. The CAS is connected to a PC through a TCP/IP network. The PC configures the CAS, displays the realtime data and stores the desired data. The system is setup to record 50 engine cycles. This provides a compromise between enough data for statistical analysis and data file size.

In order for the CAS to calculate IMEP, maximum pressure rise, start of combustion, burn duration, and peak pressure correctly the system has to know where TDC is relative to the reference signal from the encoder (1 pulse/rev). In this study TDC is determined by motoring the engine and locating the peak pressure. However, TDC does not occur at peak pressure because of heat and mass losses through the rings and valve seats. The peak pressure occurs slightly before TDC. This small angle is referred to as the Thermodynamic Loss Angle (TLA). Changes in engine speed, coolant, oil and air temperature, piston ring wear, and valve-to-seat sealing all affect the TLA. The TLA is determined by warming the engine up to operating temperature and then motoring the engine at 700RPM. Then the cylinder pressure and volume is examined, in real-time, on a log-log plot. The TLA is adjusted until the compression and expansion lines are nearly parallel to each other and the polytropic indexes are within typical values. The TLA for this study is 1.5 degrees which results in the IMEP from the CAS being approximately 1.5% higher than the IMEP calculated from the load cell (BMEP) and the friction estimate FMEP.

A.4 Equipment and Instrumentation List

Table A.3: Specialized Equipment List

Item	Make / Model	Relevant Specifications
Engine Control Module	AFS Sparrow II Engine Control Module / / 400010-5	Modified to allow multiple fuels Power: +13.8V / 1Amps
Two-stage CNG Regulator	AFS/Falcon Regulator	Reduces Pressure from 3600psi to 30-150psi
CH_4/H_2 Injector	Bosch / 0280150839	Power: +13.8V / 1Amps
Gasoline Injector	Ford / 0280155710	Power: +13.8V / 1Amps
Crankshaft Angular Position Sensor	Ford 4.0L V6 proximity sensor and pulley	Used with 36 minus 1 tooth pulley / ~7V Peak to Peak
2kW Air Heater	Omega / AHF10120	Power: 208V / 25Amps
Fuel Regulator and Fuel Pump	Ford / AHF10120	Power: +13.8V / 5Amps
Miscellaneous Power Supply	Hewlett Packard 6236B	+13.8V constant voltage Powers ECM, fuel pump and fuel injectors
Programmable Temperature Controller	ERO Electronic / SQV 173	Provides closed-loop control of intake temperature Output: 4 to 20mA
Power Controller	LZF1	Regulates power to heater Input: 4 to 20mA Output: 208V / 25Amp

Table A.4: Instrumentation List

Item	Make / Model	Relevant Specifications
Intake Pressure Validyne	Validyne / DP15 20 Carrier Demodulator / CD15	Range: 0 to 10psi Output: 0 to 10V Accuracy: 0.3% full span
Exhaust Pressure Validyne	Validyne / DP15 20 Carrier Demodulator / CD15	Range: 0 to 20psi Output: 0 to 10V Accuracy: 0.8% full span
Liquid Fuel Meter	Max Machinery piston meter / 213-300 and Transmitter / 284-512	Used with Triad Industries Meter Range: 1 to 1800ml/min Output: 0 to 10V Accuracy: 0.1%
Fuel Flow Meter	Triad Industries / TM428	Used to calculate volume flow rate from Transmitter pulses (112.25 pulse/ml)
Mass Air Flow	Siemens / HFM 62B	Range: 0 to 157g/s Output: 0 to 5.1V Accuracy: 0.05g/s
Cylinder Pressure	Kisler ThermoCOMP / 6043A60	Water Cooled piezoelectric transducer Range: 0 to 250 bar Accuracy: 0.5% full scale
Charge Amplifier	MTS Charge Amplifier / 1104CA	Converts electrostatic charge from cylinder pressure transducer to a voltage
Combustion Analysis System (CAS)	Baseline CAS / E002.0093	Used to determine various combustion parameters (real time)
Crank Angle Encoder	BEI Industrial Encoder Division/XH25D-SS-3600-T2-ABZC-7272-SM18	Two signals-0.1 deg/pulse and 360 deg/pulse (TDC) Accuracy: 0.01 deg
AFRecorder	Engine Control and Monitoring / 1200A	Analog output: 0 to 5V Range: 0.4 to 10.0 λ Accuracy: $\lambda = \pm0.009$
Intake Air Temperature	Copper /Copper-Nickel T-type Thermocouple	Mounted adjacent to intake port Range: -270 to 400°C Accuracy: 1.0°C

Item	Make / Model	Relevant Specifications
Exhaust/EGR/Heater Temperature	Kromel-Alumel K-type thermocouples	Range: -270 to 1371°C Accuracy: 2.2°C
Temperature Meter	Omega / DP462	Used to read temperature from exhaust/EGR/heater
Data Acquisition Boards	National Instruments / PCI-MIO-16E-1	Analog inputs: 8 differential Resolution: 12bit Range: ±0.05 to ±10V

Appendix B

HCCI Data

Table B.1: PRF20 Data

File Numbers (xPC / CAS)	EGR (%)	Lambda	Dilution	IMEP (bar)	NO$_x$ (g/kWhr)	CO (g/kWhr)	HC (g/kWhr)	ISFC (g/kWhr)	SOC (deg)	Burn Duration (bar/deg)	Peak Pressure (bar)
930 1	1.57	1.81	0.79	3.89	0.573	12.5	35.2	287	-0.7	3.2	43.4
934 2	1.68	1.96	0.93	3.97	0.091	13.3	34.6	260	2.9	4.2	40.8
937 3	1.77	2.10	1.06	3.88	0.043	14.1	33.0	247	4.2	6.2	37.7
939 4	1.81	2.20	1.16	3.78	0.040	15.2	32.8	247	5.0	7.4	35.6
942 5	1.96	2.36	1.31	3.62	0.040	17.1	33.0	242	6.6	8.9	32.7
945 6	2.13	2.49	1.44	3.39	0.043	24.4	34.2	250	8.2	12.4	28.1
952 7	4.43	1.78	0.81	4.00	0.163	12.1	27.5	271	0.9	3.6	42.6
955 8	2.03	1.83	0.81	3.99	0.313	11.8	27.5	274	0.3	4.1	42.8
959 9	2.34	1.99	0.97	3.96	0.053	12.3	28.6	255	3.8	4.8	39.6
1001 10	2.70	2.11	1.09	3.86	0.038	14.1	31.2	248	5.4	6.2	36.6
104 11	3.27	2.20	1.20	3.73	0.037	15.2	32.0	246	6.2	7.9	34.3
106 12	3.52	2.37	1.36	3.52	0.039	19.9	32.4	249	7.6	11.4	30.0
1010 13	4.87	1.71	0.75	3.91	1.023	10.7	30.7	287	-1.8	2.8	44.1
1013 14	5.09	1.78	0.82	3.98	0.265	10.9	27.3	270	1.5	4.0	42.0
1016 15	5.31	1.91	0.96	3.96	0.042	12.8	29.3	257	4.7	5.4	38.4
1018 16	5.56	2.05	1.09	3.86	0.035	13.8	30.6	247	6.0	6.6	35.9
1020 17	5.85	2.19	1.24	3.68	0.035	17.0	31.5	247	7.3	9.3	32.2
1023 18	5.88	2.33	1.37	3.50	0.038	20.9	32.3	247	8.3	12.4	28.8
1026 19	8.74	1.64	0.74	3.98	0.526	12.2	26.3	280	-0.9	3.1	43.9
1030 20	6.84	1.68	0.75	3.88	1.077	11.5	25.8	286	-2.2	2.6	44.2
1032 21	7.09	1.77	0.85	4.02	0.070	12.3	27.3	264	3.5	4.6	40.2
1035 22	7.09	1.86	0.94	3.98	0.036	12.5	29.1	256	5.0	5.5	38.2
1039 23	7.26	2.01	1.09	3.81	0.034	13.7	29.0	245	6.2	6.9	35.7
1041 24	7.27	2.15	1.23	3.70	0.034	16.0	29.5	245	7.0	9.7	32.4
1044 25	7.26	2.32	1.40	3.34	0.040	24.8	33.6	257	8.7	15.0	26.7

File Numbers (xPC / CAS)	EGR (%)	Lambda	Dilution	IMEP (bar)	NO$_x$ (g/kWhr)	CO (g/kWhr)	HC (g/kWhr)	ISFC (g/kWhr)	SOC (deg)	Burn Duration (bar/deg)	Peak Pressure (bar)
1048 26	9.80	1.57	0.69	3.89	1.808	10.7	25.1	291	-3.3	2.4	45.0
1051 27	9.66	1.68	0.81	4.04	0.231	10.5	25.7	265	1.6	3.9	42.2
1053 28	9.31	1.80	0.92	4.03	0.034	12.5	27.3	254	5.6	6.0	37.6
1056 29	8.90	1.97	1.09	3.83	0.032	14.4	28.9	248	7.4	8.4	33.1
1058 30	8.52	2.14	1.25	3.63	0.035	18.5	30.5	246	8.3	12.4	29.3
112 31	9.82	1.57	0.69	3.89	1.815	10.0	26.4	291	-3.3	2.2	45.1
115 32	13.57	1.51	0.70	3.94	1.692	7.9	29.8	285	-2.3	2.3	44.7
117 33	12.26	1.59	0.76	4.00	0.742	7.6	30.4	273	0.0	3.3	43.2
1110 34	12.08	1.67	0.85	4.12	0.045	8.7	32.5	257	6.5	6.0	37.2
1112 35	11.79	1.82	0.99	3.90	0.032	11.7	34.9	257	9.7	9.8	30.3
1114 36	11.41	1.91	1.09	3.84	0.031	15.3	28.5	250	8.5	9.9	31.3
1117 37	11.10	2.11	1.28	3.45	0.037	23.2	33.4	260	10.4	16.1	25.1
1120 38	14.06	1.50	0.70	4.04	1.047	11.0	23.5	277	-1.6	2.6	44.7
1122 39	14.77	1.55	0.77	4.16	0.185	11.3	24.7	265	1.9	4.1	42.6
1124 40	15.27	1.64	0.88	4.10	0.030	12.7	26.0	259	8.8	7.9	33.5
1127 41	15.41	1.71	0.96	3.98	0.030	13.7	27.0	256	9.0	10.7	31.1
1129 42	14.89	1.83	1.07	3.76	0.032	16.8	29.6	259	10.5	14.1	27.3
1132 43	16.19	1.45	0.69	4.10	0.939	10.4	23.7	278	-1.5	2.7	45.0
1135 44	17.17	1.44	0.69	4.13	0.751	10.4	22.7	273	-0.5	3.3	44.3
1137 45	17.55	1.49	0.76	4.21	0.136	11.3	24.3	264	4.0	4.9	41.0
1139 46	17.95	1.58	0.87	4.13	0.029	12.5	25.5	257	9.3	9.4	32.4
1142 47	18.02	1.66	0.97	3.89	0.031	14.8	28.2	266	10.3	14.7	27.7
1145 48	20.75	1.36	0.67	4.21	0.721	10.4	16.9	275	-0.3	3.0	44.9
1148 49	19.98	1.45	0.75	4.31	0.105	11.1	18.2	256	4.8	4.9	40.8
1150 50	20.36	1.54	0.87	4.16	0.030	12.4	20.2	259	9.5	10.3	31.6
1153 51	20.76	1.34	0.64	4.22	1.285	9.7	17.7	274	-1.0	2.7	45.6
1155 52	21.13	1.31	0.61	4.21	1.507	10.2	16.7	279	-1.3	2.4	45.9

File Numbers (xPC / CAS)	EGR (%)	Lambda	Dilution	IMEP (bar)	NO$_x$ (g/kWhr)	CO (g/kWhr)	HC (g/kWhr)	ISFC (g/kWhr)	SOC (deg)	Burn Duration (bar/deg)	Peak Pressure (bar)
1158 53	22.22	1.35	0.68	4.26	0.548	10.5	17.4	268	0.4	3.6	44.5
120 54	22.61	1.41	0.76	4.38	0.041	11.4	19.2	254	8.2	7.3	36.3
122 55	22.55	1.48	0.85	4.19	0.029	11.8	20.4	258	10.5	11.9	30.2
125 56	23.87	1.27	0.62	4.32	1.017	9.9	16.4	268	-0.2	3.1	45.5
128 57	24.46	1.31	0.67	4.36	0.362	10.5	17.7	263	2.4	3.9	43.7
1210 58	24.25	1.38	0.76	4.41	0.031	10.5	19.6	251	10.0	10.0	32.9
1214 59	25.26	1.37	0.78	4.37	0.033	10.7	20.6	256	10.5	10.7	31.7
1218 60	26.57	1.15	0.52	4.50	1.858	8.2	22.8	259	-0.1	2.5	47.1
1220 61	27.25	1.14	0.52	4.52	1.491	8.7	22.9	256	0.6	2.7	46.8
1223 62	28.38	1.19	0.61	4.53	0.382	9.6	24.6	250	3.2	3.9	44.0
1225 63	25.92	1.27	0.65	4.48	0.031	8.7	28.3	245	12.1	14.2	29.1
1232 64	29.83	1.07	0.47	4.85	0.617	7.6	20.6	224	4.5	4.0	44.7
1234 65	30.58	1.13	0.54	4.79	0.166	8.7	22.7	223	8.3	6.0	39.2
1239 66	28.82	0.97	0.27	5.29	0.131	6.9	28.5	215	13.3	9.7	33.1
1242 67	29.46	0.99	0.36	5.12	0.739	7.3	25.7	221	4.7	3.8	46.3
1245 68	30.00	1.02	0.41	5.02	0.763	6.8	20.5	216	4.5	3.9	45.6
1250 70	30.91	0.98	0.33	5.19	0.358	7.2	24.9	214	8.3	5.1	42.0

Table B.2: PRF40 Data

File Numbers (xPC / CAS)	EGR (%)	Lambda	Dilution	IMEP (bar)	NO$_x$ (g/kWhr)	CO (g/kWhr)	HC (g/kWhr)	ISFC (g/kWhr)	SOC (deg)	Burn Duration (bar/deg)	Peak Pressure (bar)
939 1	1.23	1.58	0.56	4.30	5.90	29.7	9.4	286	-0.5	2.2	46.6
943 2	1.34	1.65	0.63	4.43	1.42	30.1	10.3	266	3.5	5.1	43.0
952 4	1.31	1.64	0.62	4.40	2.22	28.5	10.6	270	2.4	5.5	43.5
957 5	1.39	1.54	0.53	4.13	8.04	29.1	9.4	300	-1.4	2.0	47.2
101 6	2.72	1.51	0.52	4.15	8.71	25.3	9.5	300	-1.9	1.8	47.7
104 7	2.66	1.58	0.58	4.26	4.66	23.2	9.6	285	-0.4	2.5	46.2
107 8	2.92	1.64	0.65	4.42	1.13	24.5	11.4	263	3.8	4.9	42.6
1017 10	4.35	1.50	0.53	4.25	6.42	27.6	8.9	290	-0.8	2.0	46.7
1019 11	5.54	1.54	0.59	4.31	3.06	26.1	10.3	280	1.2	2.7	45.1
1022 12	5.33	1.62	0.67	4.54	0.35	27.5	9.5	256	7.7	7.5	37.5
1026 13	8.06	1.43	0.52	4.30	5.23	31.0	7.9	285	-0.6	1.9	47.2
1029 14	7.32	1.50	0.58	4.34	3.00	23.1	9.2	274	0.4	2.6	45.8
1032 15	7.39	1.55	0.64	4.53	0.62	24.6	9.7	259	5.0	4.5	41.9
1038 17	8.65	1.35	0.45	4.32	9.20	24.8	7.7	294	-1.6	1.5	49.1
1040 18	10.29	1.33	0.45	4.44	8.74	23.2	7.4	283	-0.9	1.7	48.8
1043 19	10.55	1.38	0.50	4.42	5.71	23.9	8.0	279	0.0	1.9	47.4
1045 20	10.95	1.44	0.58	4.43	2.23	24.0	9.1	269	2.2	2.8	45.0
1049 22	12.79	1.29	0.44	4.61	6.22	26.5	6.3	272	0.7	1.9	48.4
1052 23	12.30	1.35	0.51	4.45	4.21	23.4	7.3	274	1.3	2.3	46.3
1055 24	12.37	1.41	0.57	4.51	1.84	23.0	8.0	266	3.0	3.3	44.3
1059 25	15.22	1.26	0.45	4.61	4.86	22.4	6.4	273	1.8	2.3	47.1
112 26	15.37	1.31	0.51	4.63	2.77	21.4	7.3	264	2.8	2.8	45.4
114 27	12.52	1.45	0.58	4.74	0.29	25.2	7.9	237	12.7	11.4	31.0
118 28	19.21	1.22	0.48	4.88	2.15	22.5	6.4	257	4.7	3.3	44.9
1140 35	17.76	1.33	0.58	4.79	0.79	22.1	8.6	252	6.8	4.4	41.6

File Numbers (xPC / CAS)	EGR (%)	Lambda	Dilution	IMEP (bar)	NO$_x$ (g/kWhr)	CO (g/kWhr)	HC (g/kWhr)	ISFC (g/kWhr)	SOC (deg)	Burn Duration (bar/deg)	Peak Pressure (bar)
1128 31	19.56	1.19	0.44	4.90	2.63	17.5	6.0	243	5.6	3.6	46.0
1132 32	19.62	1.19	0.45	4.91	2.82	19.0	7.0	259	4.5	3.0	45.7
1134 33	19.84	1.23	0.49	4.87	1.77	20.0	7.2	258	5.3	3.6	44.4
1148 36	20.48	1.14	0.40	5.07	3.03	22.5	5.6	257	5.3	3.1	45.9
1151 37	22.64	1.12	0.41	5.14	2.52	20.0	4.5	250	5.9	3.5	45.4
1153 38	22.91	1.15	0.45	5.08	1.49	20.0	5.8	250	6.6	3.7	44.0
1159 40	24.35	1.05	0.35	5.40	1.19	22.6	4.1	244	10.9	6.7	38.9
122 41	24.27	1.00	0.29	5.57	1.32	22.0	4.0	240	10.6	5.4	41.2
125 42	24.01	0.98	0.26	5.66	1.31	23.0	3.9	241	11.0	5.6	41.4
128 43	22.87	0.99	0.19	5.65	0.69	26.0	4.0	242	13.0	8.7	36.4
1212 44	23.83	1.08	0.38	5.31	1.17	21.3	4.9	241	10.0	5.6	40.0

Table B.3: PRF60 Data

File Numbers (xPC / CAS)	EGR (%)	Lambda	Dilution	IMEP (bar)	NO_x (g/kWhr)	CO (g/kWhr)	HC (g/kWhr)	ISFC (g/kWhr)	SOC (deg)	Burn Duration (bar/deg)	Peak Pressure (bar)
1131 1	1.42	1.50	0.49	4.64	7.60	55.7	11.1	295	6.0	2.8	46.1
1136 2	1.26	1.43	0.42	4.72	12.06	57.8	12.4	305	5.7	2.2	48.2
1138 3	1.34	1.49	0.48	4.78	6.61	49.5	13.2	285	7.7	3.9	44.7
1150 4	2.76	1.45	0.46	4.80	7.62	40.4	12.2	287	7.2	3.1	45.5
1152 5	3.20	1.47	0.49	4.92	4.84	36.9	12.9	278	8.6	4.1	43.6
120 6	4.39	1.47	0.51	4.98	1.71	29.4	9.4	270	11.9	8.8	37.6
122 7	6.11	1.35	0.41	4.90	10.43	28.4	8.9	288	6.3	2.5	48.0
125 8	6.03	1.42	0.48	4.90	5.27	27.1	10.1	277	8.0	3.4	44.6
128 9	6.31	1.42	0.48	4.96	5.01	26.8	9.0	273	7.7	3.6	45.2
1212 10	9.82	1.26	0.37	5.09	9.58	26.4	7.7	279	7.5	2.9	47.5
1215 11	8.06	1.30	0.38	5.00	10.69	27.3	8.5	283	6.8	2.7	47.6
1217 12	8.01	1.34	0.43	4.98	7.23	26.0	8.3	275	8.3	3.3	45.1
1219 13	8.12	1.37	0.46	5.00	4.60	26.1	8.4	273	9.4	3.9	43.2
1222 14	8.24	1.38	0.47	5.01	3.41	26.4	8.6	270	10.2	4.8	41.7
1226 15	9.75	1.27	0.37	5.15	8.91	26.2	7.5	274	8.0	3.0	46.8
1228 16	9.84	1.30	0.41	5.12	7.09	25.1	8.0	270	9.0	3.4	45.0
1230 17	10.34	1.32	0.44	5.11	4.30	24.1	8.3	270	10.4	4.4	42.2
1236 18	10.04	1.32	0.44	5.13	3.60	24.9	7.9	269	11.3	5.5	40.9
1242 19	11.90	1.15	0.28	5.34	10.27	33.2	9.7	279	10.4	3.6	46.0
1244 20	12.10	1.16	0.29	5.38	10.53	32.8	9.4	275	10.1	3.9	46.0
1247 21	12.14	1.17	0.31	5.77	6.37	22.0	5.5	251	10.2	3.8	45.4
1251 23	12.32	1.24	0.39	5.31	3.67	23.0	6.3	263	12.6	6.4	39.5
1257 24	14.17	1.05	0.20	5.83	7.24	24.4	4.4	265	13.7	4.5	42.6
131 25	14.94	1.01	0.17	5.94	5.74	25.9	4.6	266	15.3	6.4	39.9
134 26	14.81	0.99	0.15	6.08	5.64	27.2	4.9	264	14.8	5.1	42.5

File Numbers (xPC / CAS)	EGR (%)	Lambda	Dilution	IMEP (bar)	NO_x (g/kWhr)	CO (g/kWhr)	HC (g/kWhr)	ISFC (g/kWhr)	SOC (deg)	Burn Duration (bar/deg)	Peak Pressure (bar)
136 27	14.56	0.97	0.12	6.12	5.00	29.2	7.7	267	14.8	5.3	42.4
1310 28	15.20	1.08	0.25	5.73	4.68	22.3	4.7	265	15.4	7.3	37.8
1313 29	15.33	1.11	0.28	5.61	4.21	22.1	4.9	266	15.5	7.8	36.8
1318 30	12.94	0.99	0.12	5.85	8.90	37.9	5.9	277	9.7	2.8	50.7
1321 31	14.35	0.98	0.13	6.04	6.91	30.4	6.8	269	11.7	3.6	47.5
1323 32	14.35	0.95	0.09	6.11	5.10	31.7	17.6	270	12.2	4.6	46.9
1326 33	16.59	0.96	0.11	6.08	3.14	31.3	15.3	270	15.7	8.2	39.2

Appendix C

Program and Data File Summary

The following lists all data files that were used and generated over the course of this work.

C.1 xPC Data Acquisition, Data Analysis and Plotting Programs

Table C.1: xPC Data Acquisition Programs

File Name	Driver or Function	File Description
CFR_Daqpgm.mdl	Function	xPC data acquisition model
parameterfile.m	Function	Signal calibration constants
openbuild.m	Driver	Opens and builds the xPC model, and loads parameterfile
savedata.m	Driver	Runs DAQ model at specified sample rate, saves 60 seconds of data, saved file name based on time stamp
Emission_Cal_1.mdl	Function	xPC emissions calibration model
EmissionAverage.m	Driver	Used to calibrate the emissions bench, averages 20 sec of emission data and outputs voltages to screen

Table C.2: Data Analysis Programs

File Name	Driver or Function	File Description
`dataanalysis_DOWN_UP.m`	Both	Separates data into proper columns, calculates mean of parameters, λ, mass flow rates of emissions species and effective dilution
`datacompile.m`	Driver	Compiles 1st set of data (Sept. 19, 24 and 27/03), calculates all parameters and saves data points as a single summary file
`datacompile2.m`	Driver	Compiles 2nd set of data (Nov. 25, 27, 28 and Dec. 3/03)
`datacompile3.m`	Driver	Compiles 3rd set of data (Jan. 6 and 7/04)
`cas2mat2.m`	Function	Converts CAS *.PO1 data files to *.mat data files, run by data compile programs
`lambda2.m`	Function	Calculates λ, emission mass fraction, percent EGR and mass of EGR from emissions analyzers, run by `dataanalysis_DOWN_UP.m`
`MassAirCorrection.m`	Function	Corrects the mass air rate calibration constants for pre-Jan.6/04 data, run by `dataanalysis_DOWN_UP.m`
`MassFuelCorrection.m`	Function	Calculates mass fuel rate from mass air rate, EGR and λ, run by `dataanalysis_DOWN_UP.m`
`combustionanalysis2.m`	Function	Determines correct indexing for cylinder pressure, crank angle, and cylinder volume signals, run by data compile programs
`expMeanPress2.m`	Function	Calculates mean pressure signal, takes 3rd order derivative, finds POI, calculates EOC, CA10 and Burn1090 based on MFB, run by `combustionanalysis2.m`
`pressFilt2.m`	Function	Filters cylinder pressure signal with a low pass 4th order filter, run by `expMeanPress2.m`

Table C.3: Plotting Programs

File Name	Driver or Function	File Description
`cont_plot.m`	Function	Creates contour plots of parameters as a function of percent EGR and λ
`cont_plot_new.m`	Function	Creates contour plots using a specified rotated x-axis
`cont_plot_par.m`	Function	Creates contour plots using specified parabolic function
`n80hep20oct.m`	Driver	Plots PRF20 for 2nd set of data
`n60hep40oct.m`	Driver	Plots PRF40 for 2nd set of data
`n40hep60oct.m`	Driver	Plots PRF60 for 2nd set of data
`j80hep20oct.m`	Driver	Plots PRF20 for 3rd set of data
`j60hep40oct.m`	Driver	Plots PRF40 for 3rd set of data
`j40hep60oct.m`	Driver	Plots PRF60 for 3rd set of data
`trendplotting`	Driver	Plots miscellaneous parameters
`vect_all_v2.m`	Driver	Plots NO_x, ON, and peak pressure correlation